NACA TN No. 1738

8186

TECH LIBRARY KAFB, NM
0144922

NATIONAL ADVISORY COMMITTEE FOR AERONAUTICS

TECHNICAL NOTE

No. 1738

WIND-TUNNEL INVESTIGATION AT LOW SPEED OF THE LATERAL CONTROL CHARACTERISTICS OF AILERONS HAVING THREE SPANS AND THREE TRAILING-EDGE ANGLES ON A SEMISPAN WING MODEL

By Leslie E. Schneiter and Rodger L. Naeseth

Langley Aeronautical Laboratory
Langley Field, Va.

Washington
November 1948

TECH

TECH LIBRARY KAFB, NM
0144922

NATIONAL ADVISORY COMMITTEE FOR AERONAUTICS

TECHNICAL NOTE NO. 1738

WIND-TUNNEL INVESTIGATION AT LOW SPEED OF THE LATERAL CONTROL CHARACTERISTICS OF AILERONS HAVING THREE SPANS AND THREE TRAILING-EDGE ANGLES ON A SEMISPAN WING MODEL

By Leslie E. Schneiter and Rodger L. Naeseth

SUMMARY

A wind-tunnel investigation has been made of the low-speed lateral control characteristics of a tapered, low-drag, semispan wing model equipped with 20-percent-chord sealed ailerons having spans of 0.954, 0.583, and 0.294 percent of a full-span aileron, each with trailing-edge angles of 6°, 14°, and 25°. The investigation also included tests with the ailerons unsealed, simulating symmetrical lift-flap configurations having spans of 0.954 and 0.660 percent of a full-span flap. The aileron hinge-moments and pressures over the aileron seal were determined for each of the nine aileron configurations in addition to the usual lift and lateral-control coefficients.

The results of this investigation, in general, indicated that the existing theoretical method for predicting the slope of the curve of rolling-moment coefficient with aileron deflection $C_{l_{\delta_a}}$ for various spans of aileron gave satisfactory agreement with the experimental results for ailerons having trailing-edge angles of 6° and 14°. The agreement between the experimental and theoretical values of $C_{l_{\delta_a}}$ was poor, however, for the ailerons with a trailing-edge angle of 25°.

The existing empirical relationships for predicting the incremental change in the slope of the curves of aileron hinge-moment coefficient with both aileron deflection $C_{h_{\delta_a}}$ and wing angle of attack C_{h_α} resulting from an incremental change in the aileron trailing-edge angle may be used satisfactorily to estimate the effects of variation of the control-surface trailing-edge angle regardless of the span of the control surface. For a constant aileron trailing-edge angle, the variation with increasing aileron span of the hinge-moment parameters was small but the parameters tended to become more positive (or less negative) with decrease in aileron span.

INTRODUCTION

The National Advisory Committee for Aeronautics has been investigating the effects of sweepback on the rolling and lift effectiveness of various control surfaces and flaps on swept back wings. As a basis upon which to compare the results of tests of various swept-wing models, a systematic investigation was made in the Langley 300 MPH 7- by 10-foot tunnel to determine the effects of variation of aileron span and trailing-edge angle on the effectiveness and hinge-moment characteristics of 20-percent-chord sealed ailerons on an essentially unswept wing (wing leading edge sweptback 6.3°). In addition, the data were used to check the validity of various theoretical and empirical methods of calculating control-surface effectiveness and hinge-moment characteristics.

The data presented and discussed are the results of low-speed lateral-control tests of nine different 20-percent-chord sealed aileron configurations (three spans each with three trailing-edge angles) on a tapered, low-drag, semispan wing model. The rolling-moment and yawing-moment characteristics, as well as the hinge-moment and seal-pressure characteristics, of each of the aileron configurations, are presented for a range of angle of attack and aileron deflection. The characteristics of the wing in pitch, with two different spans of aileron to simulate symmetrical lift-flap configurations, were also determined and the results are presented.

COEFFICIENTS AND SYMBOLS

The forces and moments measured on the wing are presented about the wind axes which, for the conditions of these tests (zero yaw), correspond to the stability axes. The X-axis is in the plane of symmetry of the model and is parallel to the tunnel free-stream air flow. The Z-axis is in the plane of symmetry of the model and is perpendicular to the X-axis. The Y-axis is mutually perpendicular to the X- and Z-axes. All three axes intersect on the chord plane at the model plane of symmetry and at the 28.2-percent-chord station at the root of the model. (See fig. 1).

Rolling-moment and yawing-moment coefficients presented represent the aerodynamic moments on a complete wing produced by the deflection of the aileron on only the left semispan of the wing. The lift, drag, and pitching-moment coefficients represent the aerodynamic forces resulting from the deflection in the same direction of the ailerons on both semispans of the complete wing.

C_L lift coefficient $\left(\frac{\text{Twice lift of semispan model}}{qS}\right)$

ΔC_L increment of lift coefficient

C_D drag coefficient (D/qS)

C_m pitching-moment coefficient $\left(\frac{\text{Twice pitching moment of semispan model}}{qS\bar{c}}\right)$

C_l rolling-moment coefficient (L/qSb)

C_n yawing-moment coefficient (N/qSb)

C_h aileron hinge-moment coefficient $(H_a/2qM)$

P seal-pressure coefficient, ratio of difference between pressures below and above seal divided by free-stream dynamic pressure; subscripts 1, 2, 3, . . . indicate stations at which pressure measurements are made (fig. 2)

D twice drag of semispan model

L rolling moment due to aileron deflection about X-axis, foot-pounds

N yawing moment due to aileron deflection about Z-axis, foot-pounds

H_a aileron hinge moment, foot-pounds

q free-stream dynamic pressure, pounds per square foot $\left(\frac{1}{2}\rho V^2\right)$

S twice area of semispan wing model, 17.54 square feet

b twice span of semispan model, 10.48 feet

A aspect ratio of wing, 6.23 $\left(\frac{b^2}{S}\right)$

$\bar{c}$ wing mean aerodynamic chord, 1.745 feet $\left(\frac{2}{S}\int_0^{b/2} c^2\,dy\right)$

c local wing chord, feet

M area moment of aileron behind and about the hinge axis, feet^3

$\bar{x}$ distance along X-axis from leading edge of root chord to leading edge of mean aerodynamic chord, 0.254 foot $\left(\frac{2}{S}\int_0^{b/2} cx\,dy\right)$

b_a span of aileron or flap, measured parallel to Y-axis, feet

b_a' span of full-span aileron or flap, measured parallel to Y-axis, feet

y lateral distance from plane of symmetry, measured parallel to Y-axis, feet

x longitudinal distance from leading edge of wing-root chord to wing leading edge, measured parallel to X-axis, feet

V free-stream velocity, feet per second

ρ mass density of air, slugs per cubic foot

α angle of attack of wing with respect to chord plane at root of model, degrees

δ_a aileron-deflection angle relative to chord plane of wing, measured in a plane perpendicular to aileron-hinge axis and positive when trailing edge is down, degrees

ϕ aileron trailing-edge angle, measured in a plane perpendicular to aileron hinge axis, degrees

$C_l/\Delta\alpha$ rolling-moment coefficient produced by 1° difference in angle of attack of various right and left parts of a complete wing (reference 1)

α_δ effective change in angle of attack over flapped part of a wing produced by a unit change in flap deflection

$C_{h_\alpha} = \left(\frac{\partial C_h}{\partial \alpha}\right)_{\delta_a}$

$$C_{h_{\delta_a}} = \left(\frac{\partial C_h}{\partial \delta_a}\right)_\alpha$$

$$C_{L_\alpha} = \left(\frac{\partial C_L}{\partial \alpha}\right)_{\delta_a}$$

$$C_{l_{\delta_a}} = \left(\frac{\partial C_l}{\partial \delta_a}\right)_\alpha$$

$$P_{\delta_a} = \left(\frac{\partial P}{\partial \delta_a}\right)_\alpha$$

The subscripts δ_a and α outside the parenthesis indicate the factor held constant. All slopes were measured in the vicinity of 0° angle of attack and 0° aileron deflection.

CORRECTIONS

The values of C_D, C_l, C_n, and α presented have been corrected for jet-boundary and reflection-plane effects. Blockage corrections to account for the constriction effects of the wing model and wing wake have been applied to the data.

No corrections have been applied to the data to account for the small amount of wing twist produced by aileron deflection or for the tare effects of the root fairing.

APPARATUS AND MODEL

The semispan model was mounted vertically in the Langley 300 MPH 7- by 10-foot tunnel, as shown in figure 3. The root chord of the model was adjacent to the ceiling of the tunnel, the ceiling of the tunnel thereby serving as a reflection plane. The model was mounted on the six-component balance system in such a manner that all forces and moments acting on the model could be measured. A small clearance was maintained between the model and the tunnel ceiling so that no part of the model came in contact with the tunnel wall. A root fairing, consisting of a body of revolution, was attached to the root of the model in order to deflect the spanwise flow of air (through the clearance hole between the model and the tunnel ceiling) into the tunnel test section and to minimize the effects of any such inflow on the flow over the wing model.

The model was constructed of laminated mahogany over a welded-steel framework to the plan-form dimensions shown in figure 1. The model had wing sections of NACA 65_1-012 profile perpendicular to the 50-percent-chord line with neither twist nor dihedral, an aspect ratio of 6.23, and a taper ratio of 0.49.

Transition was fixed at the leading edge of the wing for all tests. The transition strip, consisting of No. 60 carborundum grains, extended over the forward 5 percent of the wing chord on both the upper and lower surface along the entire span of the wing model. The carborundum grains were sparsely spread to cover from 5 to 10 percent of this area.

The semispan wing model was equipped with 20-percent-chord ailerons normal to the wing 50-percent-chord line. The three aileron profiles shown in figure 4 were used to obtain trailing-edge angles of 6° (true-contour trailing edge of NACA 65_1-012 airfoil), 14° (flat-sided from aileron hinge line to trailing edge of wing), and 25° (beveled trailing edge). Each aileron had a steel spar and was constructed with joints at two spanwise stations so that aileron spans of $0.294b_a'$, $0.583b_a'$, and $0.954b_a'$ could be tested (fig. 1). Two aileron configurations ($b_a = 0.660b_a'$ and $0.954b_a'$) were deflected to simulate symmetrical lift flaps. The area moments of the various spans of aileron and lift flap are given in the following table:

b_a/b_a'	M (ft^3)
0.954	0.2770
.583	.1238
.294	.0472
.660	.2300

During tests with the partial-span ailerons, the undeflected part of the wing trailing edge was equipped with the true-contour-aileron profile ($\phi = 6°$). For all of the tests except lift-flap tests, the aileron was sealed with a plastic impregnated cloth seal across the gap ahead of the aileron nose, except at the point of attachment of the aileron actuating mechanism and at the aileron support bearings. The seal extended and was attached to the bearing housings at the end of each aileron-seal chamber, and it is believed that the seal in each chamber was fairly complete. Pressure orifices were located above and below the seal in the wing block ahead of the aileron at the spanwise stations shown in figure 2. Two pairs of pressure orifices were located in each of the aileron sections.

A remotely controlled, motor-driven, aileron-actuating mechanism was used to obtain the various aileron deflections employed in the investigation. The aileron angles were constantly indicated on a meter by the

use of a calibrated potentiometer which was mounted on the aileron-hinge axis near the outboard end of the aileron. A calibrated electrical-resistance-type strain gage was employed to measure the aileron-hinge moments.

TESTS

All the tests were performed at an average dynamic pressure of approximately 20.5 pounds per square foot, which corresponds to a Mach number of 0.12 and a Reynolds number of 1,500,000 based on a mean aerodynamic chord of 1.75 feet.

Lift-flap tests with the maximum span aileron, unsealed, ($b_a = 0.954b_a'$, $\phi = 14^\circ$) and with the two inboard aileron sections, also unsealed, ($b_a = 0.660b_a'$, $\phi = 14^\circ$) at deflections of 0°, 10°, 20°, 30°, 40°, 50°, and 60° were performed through an angle-of-attack range from -6° to the wing stall.

Lateral-control tests with the nine different combinations of aileron span and trailing-edge angle, were performed through an aileron-deflection range from -30° to 30° with the constant angle of attack varied from -4° to 12° in increments of 4°. The aileron was sealed for all of the lateral-control tests.

RESULTS AND DISCUSSION

Presentation of Data

The results of the lift-flap tests of the wing with the unsealed aileron at deflections from 0° to 60° are presented in figure 5 for the $b_a = 0.954b_a'$ flap and in figure 6 for the $b_a = 0.660b_a'$ inboard flap. The lift-coefficient increments produced by both flaps at various deflections are shown in figure 7. The variation of the aileron lateral control characteristics (rolling-moment, yawing-moment, hinge-moment, and seal-pressure coefficients) with aileron deflection at various angles of attack for each of the combinations of aileron span and trailing-edge angle are shown in figures 8 to 16. The lateral-control parameters $C_{l_{\delta_a}}$, $C_{h_{\delta_a}}$, and C_{h_α} as determined from these tests, are shown plotted against relative position of the inboard end of the aileron in figure 17 and against aileron trailing-edge angle in figure 18. The experimental values of $\Delta C_{h_{\delta_a}}$ and ΔC_{h_α} (the increments of $C_{h_{\delta_a}}$ or C_{h_α} resulting from an incremental change in trailing-edge angle) are compared in figure 19 with the empirical relations given in reference 2. Values of the total rolling-moment coefficient produced by ±30° aileron deflection, and values of the seal-pressure-coefficient parameter P_{δ_a} at each of the spanwise stations,

along with the aforementioned lateral-control parameters are presented in table I.

Discussion

Lift-flap tests.- For both flap configurations, the wing had a stable variation of pitching-moment coefficient with lift up to and through the stall and the wing longitudinal stability increased with flap deflection in the low-lift range. The wing, however, became approximately neutrally stable in the high-lift range at high flap deflections. Each additional increment of flap deflection produced a proportionally smaller increment of both lift and negative pitching-moment coefficient. (See figs. 5 to 7.) The type of variation of lift-coefficient increment with flap deflection shown in figure 7 is typical for most types of lift flap. The maximum values of ΔC_L produced by both spans of flaps were in excellent agreement with the data shown in reference 3 for plain flaps on an untapered wing.

Rolling-moment characteristics.- In general, the total rolling-moment coefficient for $\delta_a = \pm 30^\circ$, of all of the ailerons was relatively uneffected by angle of attack up to approximately $\alpha = 8.5^\circ$. Increasing the angle of attack to approximately 12.7°, however, resulted in a large drop (approximately 30 percent) in the total rolling-moment coefficient. (See figs. 8 to 16 and table I.)

The slope of the curve of rolling-moment coefficient against aileron deflection was fairly linear through a range of aileron deflection from -15° to 15° and was negligibly affected by wing angle of attack within a range from -4.3° to 8.5°.

The variation of $C_{l_{\delta_a}}$ with aileron span as determined by the method of reference 1 is compared with the experimentally determined values of $C_{l_{\delta_a}}$ in figure 17. The values of $C_l/\Delta\alpha$ used in the determination of the theoretical curve were taken from reference 1 and the value of α_δ (0.44 for a 0.20-chord flap) was taken from reference 2. The agreement is very good for the flaps with trailing-edge angles of 6° and 14°, but is poor for the flaps with the 25° trailing-edge angle.

Yawing-moment characteristics.- The total yawing-moment coefficient resulting from equal up and down deflection of the ailerons was approximately zero at small angles of attack ($\pm 4^\circ$), but became adverse (sign of yawing moment opposite to sign of rolling-moment) at the higher angles of attack (8° to 12°) for all combinations of aileron span and trailing-edge angle. (See figs. 8 to 16.)

Aileron hinge-moment characteristics.- Hinge-moment-coefficient data obtained for the various ailerons (figs. 8 to 16) indicated, in general, a linear variation of C_h with aileron deflection for the three aileron

spans tested with both the 6° and 14° trailing-edge angles throughout the angle-of-attack range. The variation of C_h with both aileron deflection and wing angle of attack was decidedly nonlinear for all three aileron spans with the 25° trailing-edge angle. For a constant aileron trailing-edge angle, the value of total hinge-moment coefficient resulting from ±30° deflection of the aileron was approximately constant for the three aileron spans at comparable angles of attack. For a given span of aileron, the total hinge-moment coefficient resulting from ±30° deflection of the aileron decreased as the aileron trailing-edge angle increased.

The values of the aileron hinge-moment-coefficient parameter $C_{h_{\delta_a}}$ for a constant aileron trailing-edge angle exhibited a slight shift to less negative values, and C_{h_α} for constant trailing-edge angle exhibited a negligible change as the aileron span decreased. (See figs. 17 and 18.) For a constant aileron span, both hinge-moment parameters exhibited a large change toward less negative (or more positive) values as the aileron trailing-edge angle was increased from 6° to 25°.

The experimentally determined increments of $C_{h_{\delta_\alpha}}$ and C_{h_α} are compared in figure 19 with the empirically determined curves of reference 2. The comparison indicates that the empirical relations of reference 2 predict satisfactorily the effects on the hinge-moment parameters of an incremental change in control-surface trailing-edge angle since the deviation of the experimental data from the empirical curve is of about the same order of magnitude as the deviation of the experimental data used to determine the empirical curve. In addition, the experimental data indicate that the incremental effects on the hinge-moment parameters of an incremental change in the control-surface trailing-edge angle are independent of the span of the control surface and that the empirical relationships of reference 2 may thus be used to estimate the effects of variation of the trailing-edge angle regardless of the span of the control surface.

Seal-pressure characteristics.- In general, the variation of seal-pressure coefficient with aileron deflection was quite linear for a deflection range of ±15°. (See figs. 8 to 16.) At deflections greater than ±15°, however, the slope of the curves of P with δ_a decreased, in some instances reversing, particularly, at -4.3° angle of attack. As the angle of attack increased, the slope of P against δ_a at deflections greater than ±15° approached the value obtained for the lower deflections. Increasing the wing angle of attack had little or no effect upon the slope of P with δ_a at low deflections but resulted in a slight shift of the curves toward more positive values of P.

Decreasing the aileron span, or increasing the aileron trailing-edge angle had a tendency to reduce the slope of P against δ_a (P_{δ_a} in table I) obtained at any given pressure-orifice location.

The trends of P_{δ_a} with decreasing aileron span or increasing aileron trailing-edge angle were similar to the trends of the hinge-moment parameters with variation of these same geometric characteristics.

CONCLUSIONS

The following conclusions are indicated from the results of a wind-tunnel investigation at low speeds of the lateral control characteristics of nine different 20-percent-chord sealed plain aileron configurations (three aileron spans each with three trailing-edge angles) and the characteristics of ailerons of two spans deflected to simulate symmetrical lift-flap configurations on a tapered, low-drag, semispan wing having a leading-edge-sweepback angle of 6.3°:

1. For the simulated lift-flap configurations, ailerons of both 0.660 and 0.954 span were effective in producing lift up to the maximum deflection tested (60°). Each successive increment of flap deflection, however, produced a progressively smaller increment of lift coefficient.

2. The agreement between the theoretical and experimental variation of the aileron effectiveness parameter $C_{l_{\delta_a}}$ with aileron span was good for the ailerons with trailing-edge angles of 6° and 14° but was poor for the ailerons with the trailing-edge angle of 25°. The aileron effectiveness parameter $C_{l_{\delta_a}}$ increased with increasing aileron span and with decreasing aileron trailing-edge angle.

3. In general, for the 6° and 14° trailing-edge angles, a linear variation of aileron hinge-moment coefficient with aileron deflection was obtained for ailerons of any of the three aileron spans tested. For the 25° trailing-edge angle, the variation of aileron hinge-moment coefficient with both angle of attack and aileron deflection was decidedly nonlinear.

4. The existing empirical relationships for predicting the incremental change in the slope of the curves of aileron hinge-moment coefficient with both aileron deflection $C_{h_{\delta_a}}$ and wing angle of attack C_{h_α} resulting from an incremental change in the aileron trailing-edge angle may be used satisfactorily to estimate the effects of variation of the control-surface trailing-edge angle regardless of the span of the control surface.

5. For a constant aileron trailing-edge angle, the variation with increasing aileron span of the hinge-moment parameters was small but the parameters tended to become more positive (or less negative) with decrease in aileron span.

6. In general, for all aileron spans and trailing-edge angles, the variation of the internal-seal-pressure coefficients with aileron deflection was linear for a deflection range of $\pm 15^{\circ}$. Decreasing the aileron span or increasing the aileron trailing-edge angle had a tendency to reduce the slope of the curve of seal-pressure coefficient against aileron deflection P_{δ_a} for any given seal-pressure orifice.

Langley Aeronautical Laboratory
National Advisory Committee for Aeronautics
Langley Field, Va. August 18, 1948

REFERENCES

1. Weick, Fred E., and Jones, Robert T.: Résumé and Analysis of N.A.C.A. Lateral Control Research. NACA Rep. No. 605, 1937.

2. Langley Research Department (Compiled by Thomas A. Toll): Summary of Lateral-Control Research. NACA TN No. 1245, 1947.

3. House, R. O.: The Effects of Partial-Span Plain Flaps on the Aerodynamic Characteristics of a Rectangular and a Tapered Clark Y Wing. NACA TN No. 663, 1938.

TABLE I

SUMMARY OF LATERAL CONTROL CHARACTERISTICS OF 20-PERCENT-CHORD AILERONS OF VARIOUS SPANS ON 6.3° WING

Aileron span (b_a/b_a')	ϕ (deg)	$C_{l_{\delta_a}}$	$C_{h_{\delta_a}}$	C_{h_α}	P_{δ_a}						Total C_l for $\delta_a = \pm 30°$		
					Station 1	Station 2	Station 3	Station 4	Station 5	Station 6	$\alpha = 0°$	$\alpha = 4.3°$	$\alpha = 12.7°$
0.95	6	0.00300	-0.0129	-0.0047	0.047	0.055	0.059	0.058	0.049	0.055	0.1248	0.1200	0.0888
.95	14	.00290	- .0106	- .0023	.045	.057	.057	.055	.053	.057	.1188	.1131	.0798
.95	25	.00248	- .0048	.0045	.042	.052	.052	.048	.045	.046	.1115	.1133	.0815
.58	6	.00225	- .0123	- .0053	----	----	.045	.051	.048	.054	.0945	.0930	.0696
.58	14	.00215	- .0104	- .0030	----	----	.049	.049	.048	.052	.0990	.0882	.0658
.58	25	.00183	- .0043	.0034	----	----	.040	.044	.045	.047	.0882	.0831	.0631
.29	6	.00100	- .0116	- .0050	----	----	----	----	.040	.049	.0450	.0441	.0329
.29	14	.00093	- .0101	- .0028	----	----	----	----	.040	.054	.0420	.0436	.0334
.29	25	.00083	- .0035	.0037	----	----	----	----	.041	.047	.0417	.0400	.0305

NACA

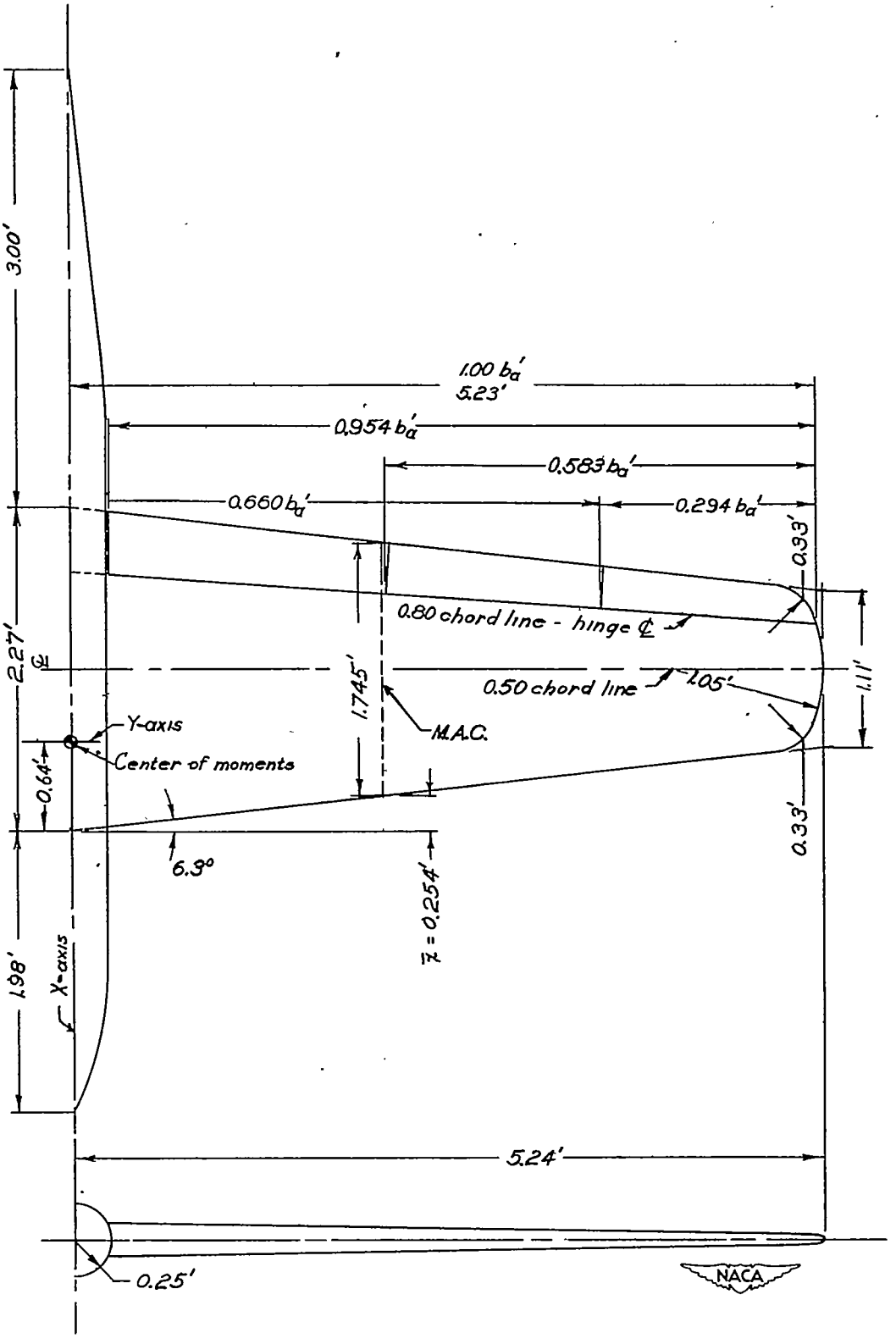

Figure 1.- Sketch of semispan wing model. S = 17.54 square feet; A = 6.23; taper ratio = 0.49. (All dimensions are in ft except as noted.)

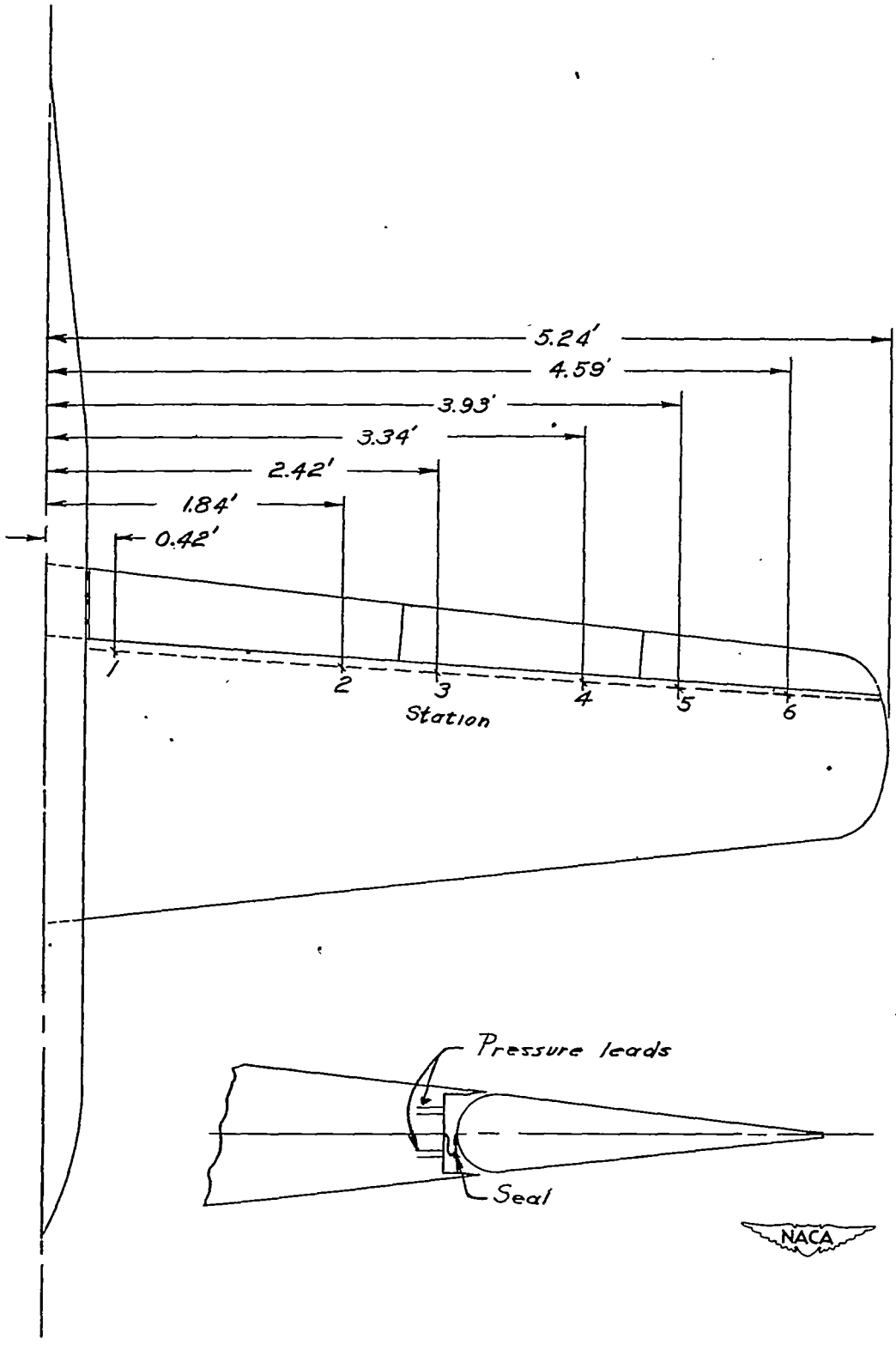

Figure 2.- Location of pressure orifices on semispan wing model. (All dimensions are in ft.)

Figure 3.- Semispan wing model mounted in Langley 300 MPH 7- by 10-foot tunnel.

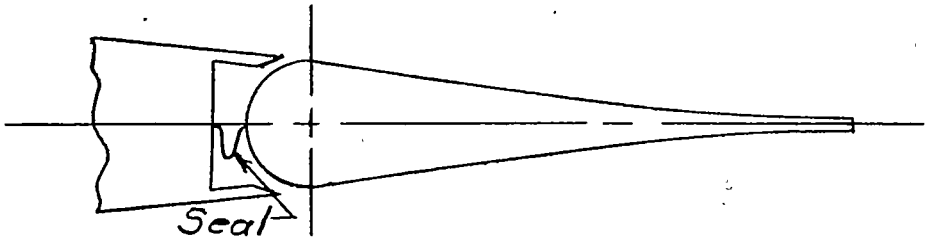

True-contour aileron (NACA 65_1-012 airfoil section), $\phi = 6°$

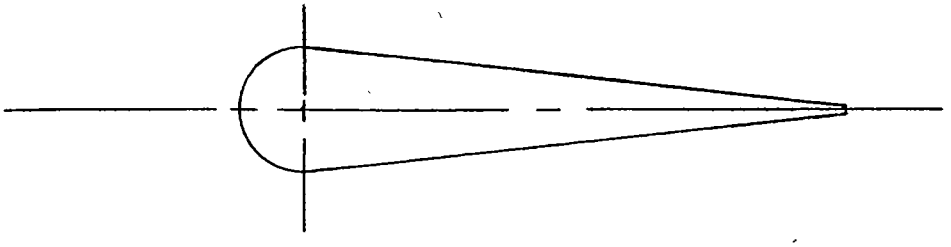

Straight-side aileron, $\phi = 14°$

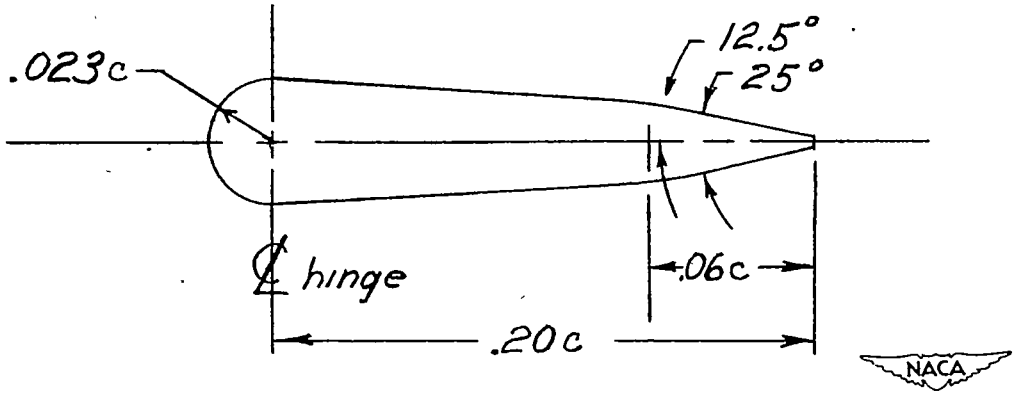

Beveled trailing-edge aileron, $\phi = 25°$

Figure 4.- Sketch of aileron contours tested on semispan wing model. (Contours and dimensions shown are in a plane perpendicular to aileron hinge line.)

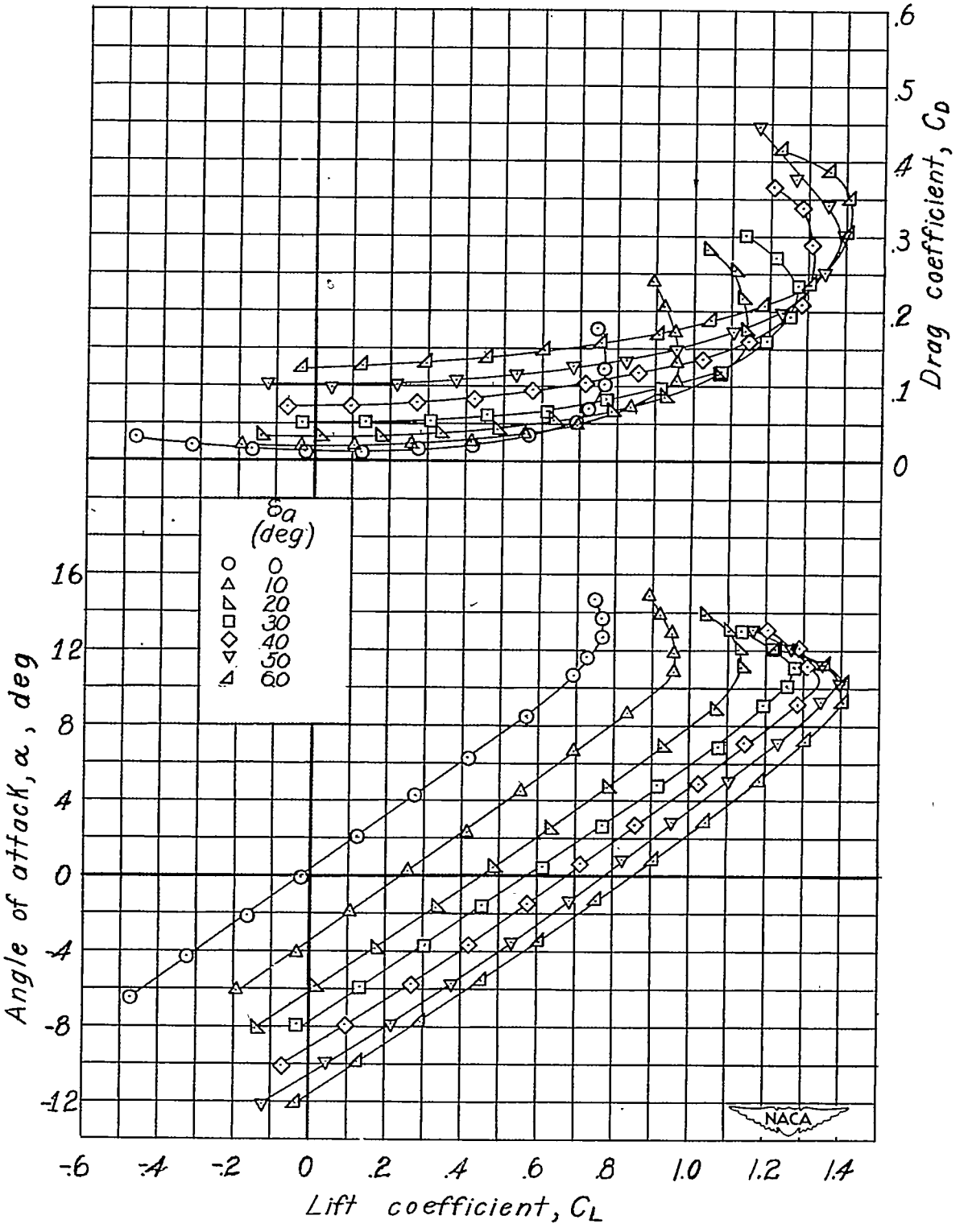

Figure 5.- Wing aerodynamic characteristics in pitch for various flap deflections. Aileron unsealed; $b_a = 0.95b_a'$; $\phi = 14^\circ$.

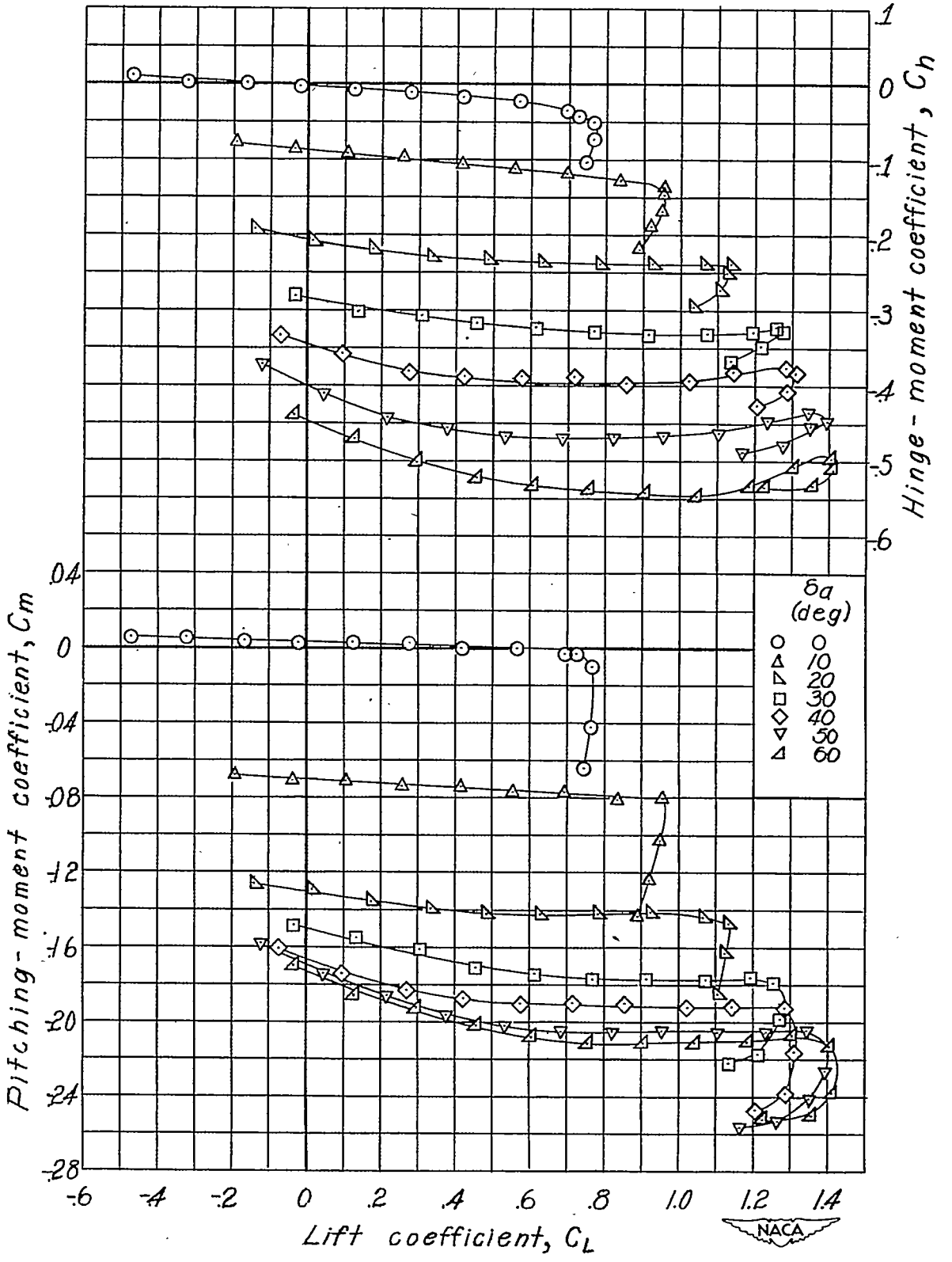

Figure 5.- Concluded.

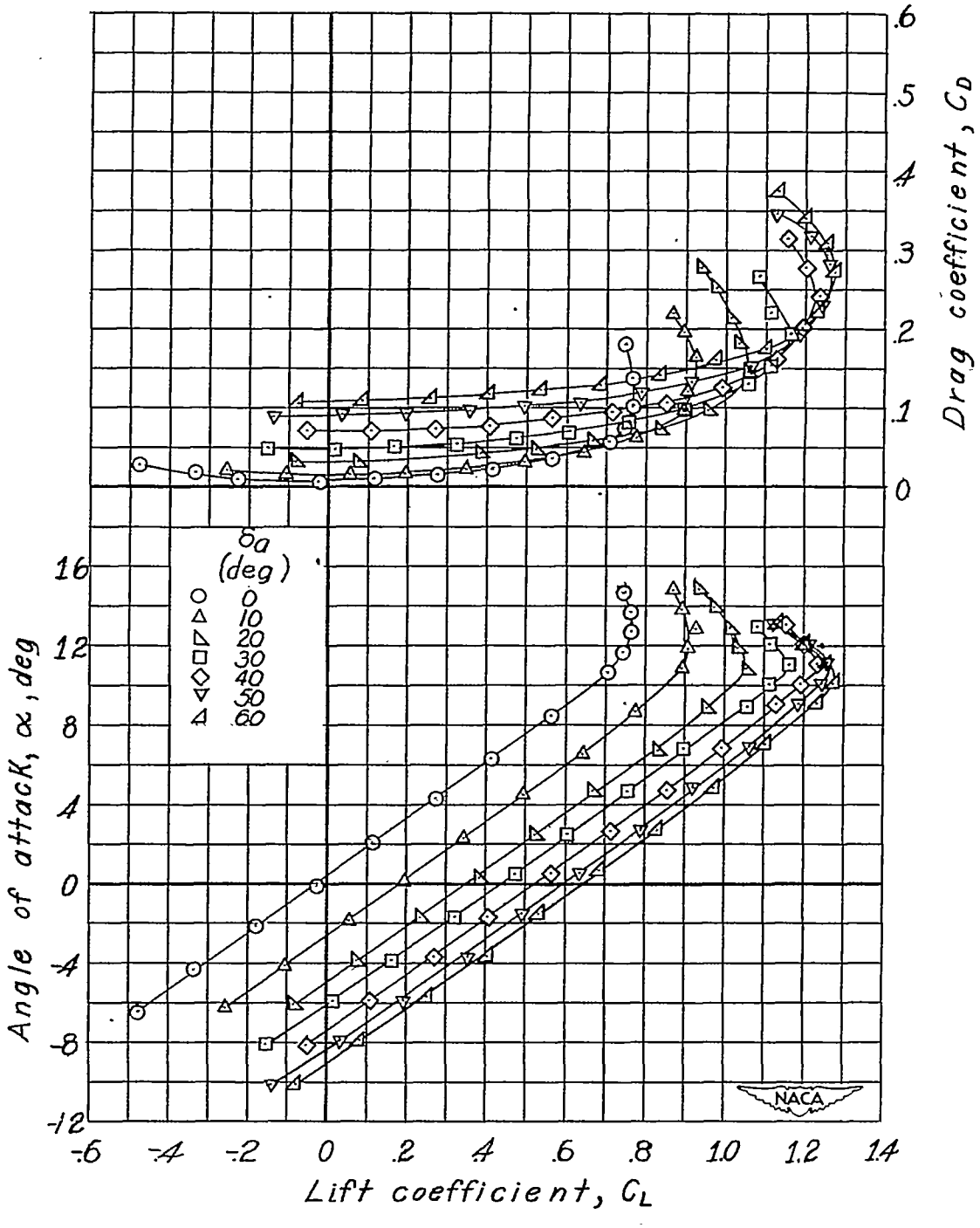

Figure 6.- Wing aerodynamic characteristics in pitch for various flap deflections. Aileron unsealed; $b_a = 0.66b_a'$; $\emptyset = 14^o$.

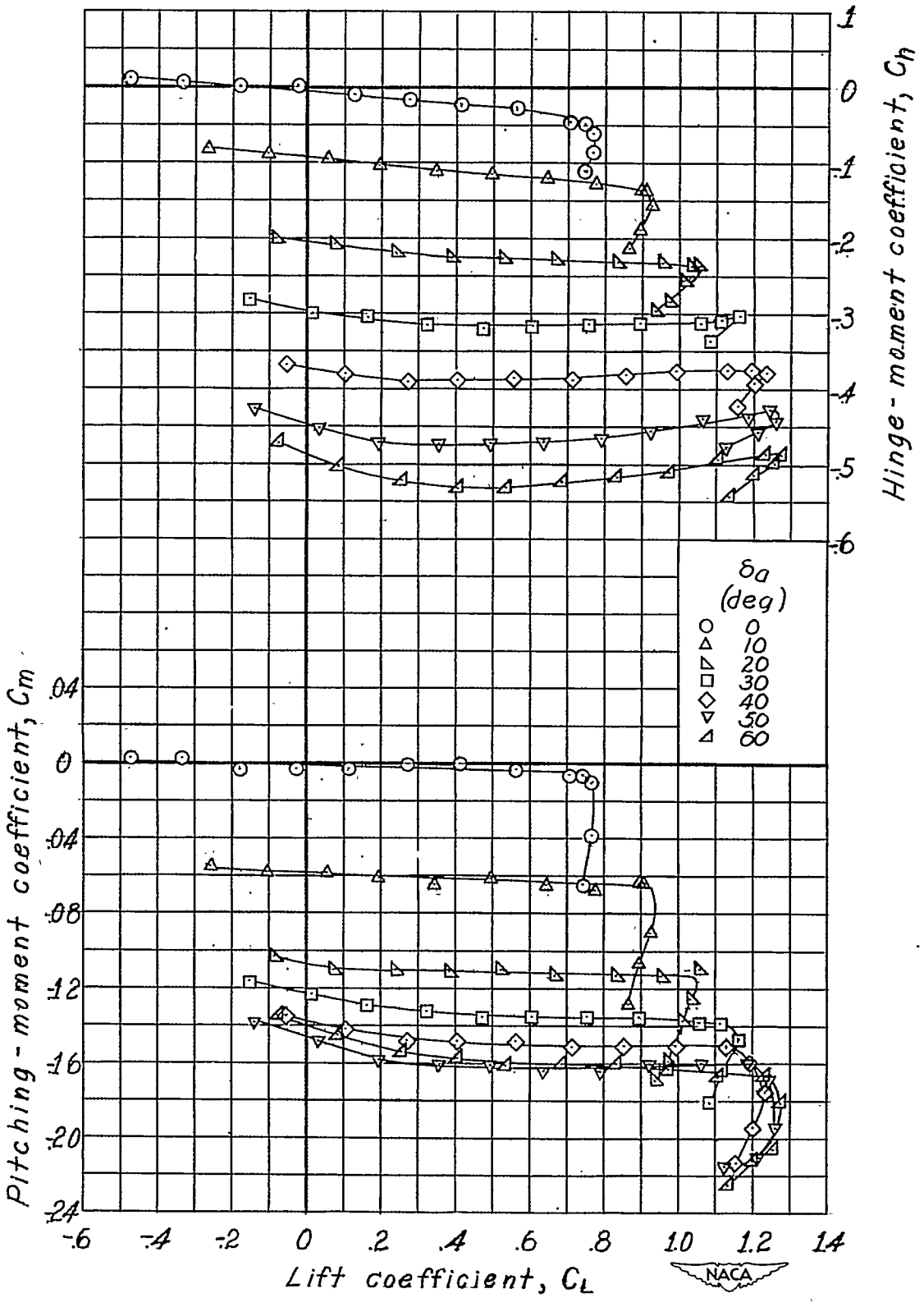

Figure 6.- Concluded.

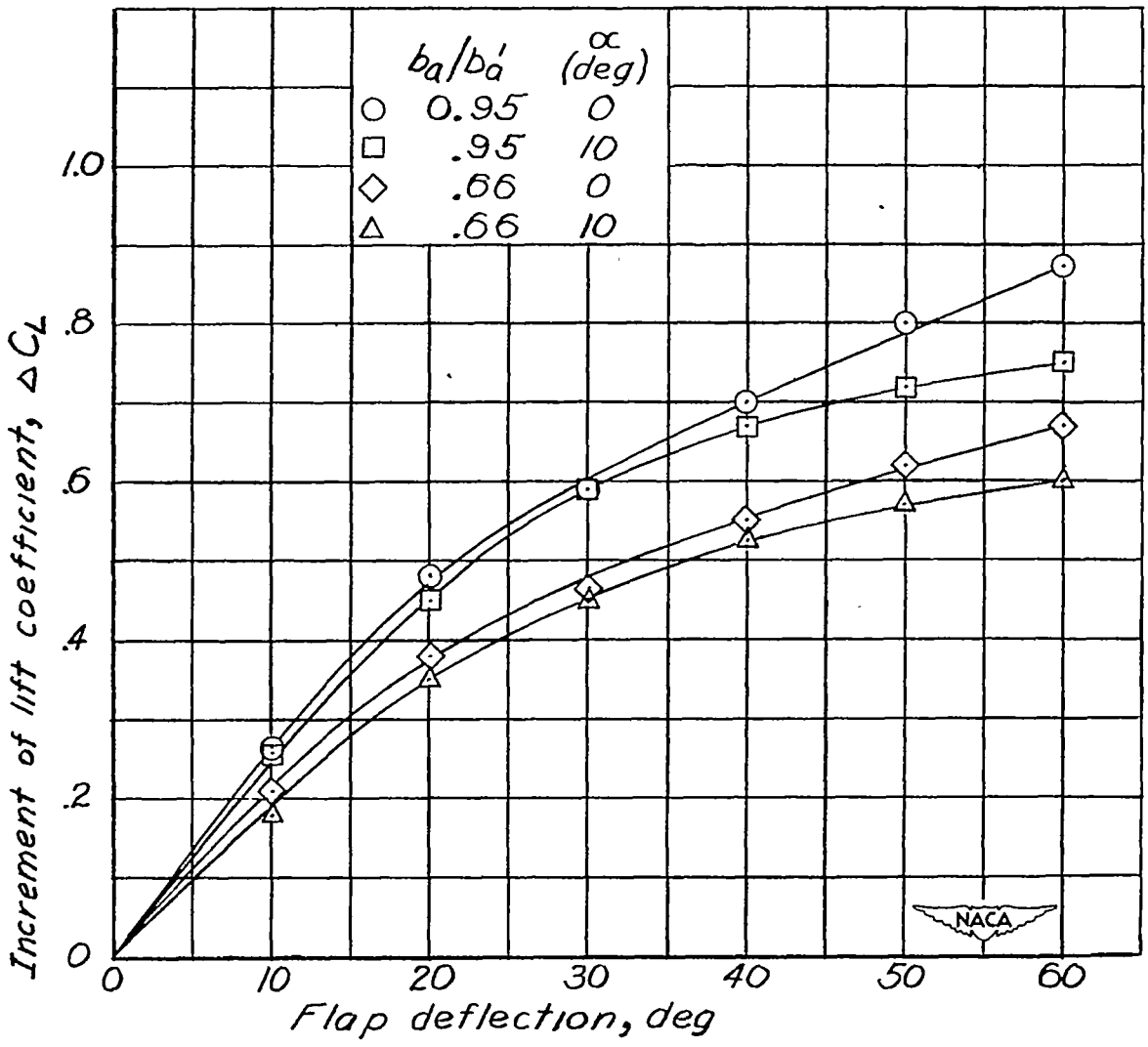

Figure 7.- Increments of lift coefficient produced by deflection of unsealed 20-percent-chord plain flaps.

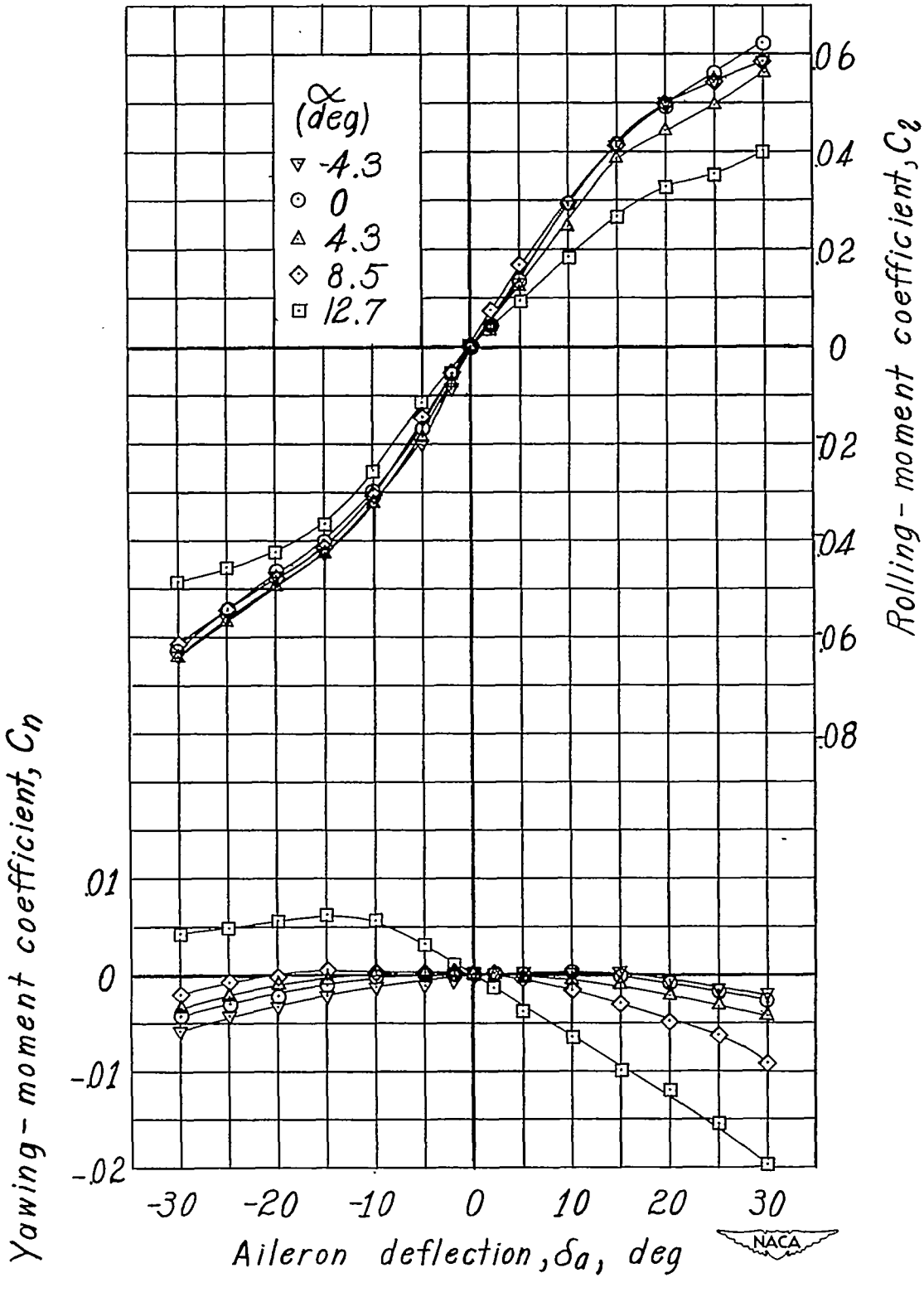

(a) Yawing- and rolling-moment coefficients.

Figure 8.- Variation of lateral control characteristics with aileron deflection. Aileron sealed; $b_a = 0.95b_a'$; $\emptyset = 6^o$.

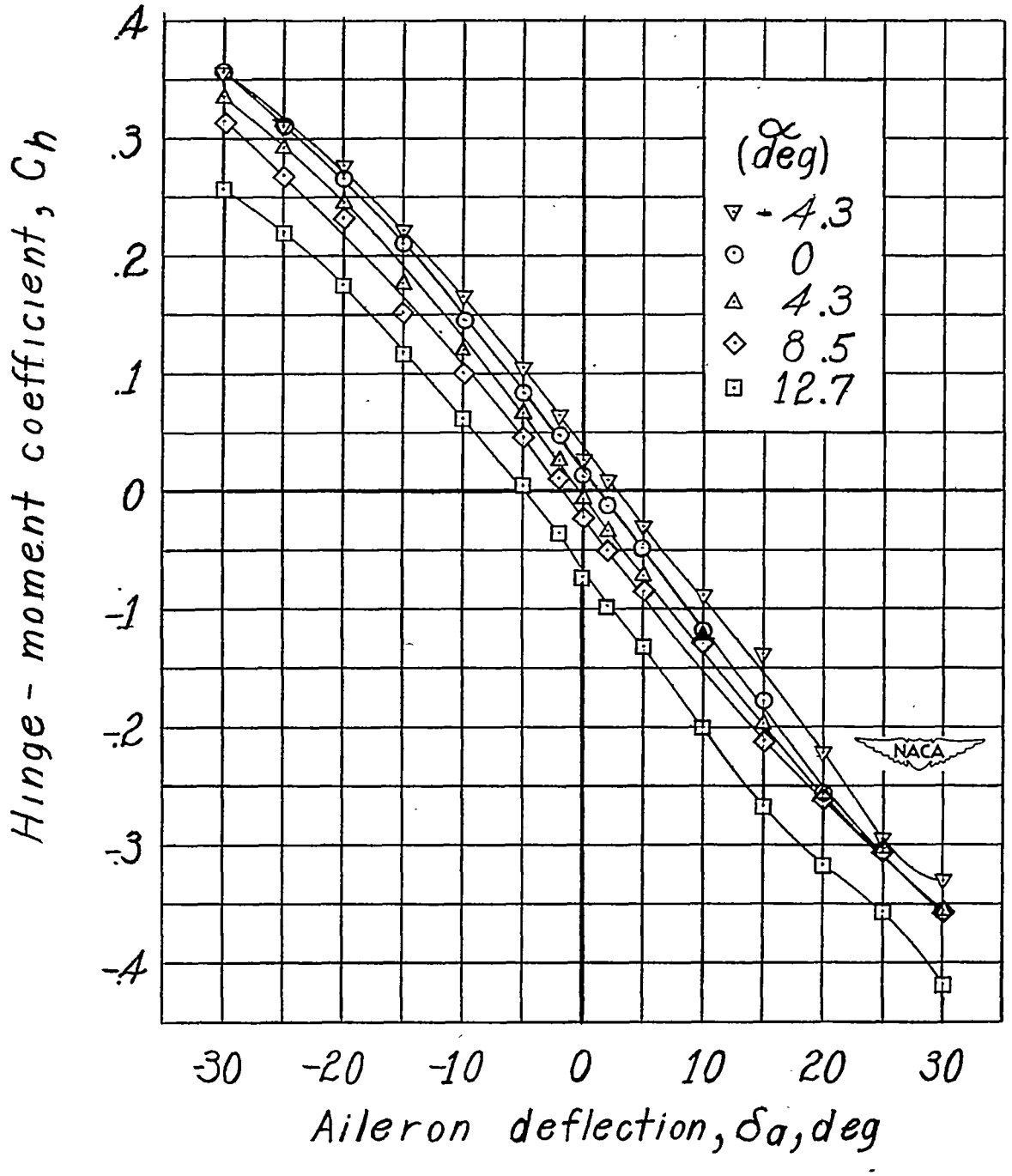

(b) Hinge-moment coefficient.

Figure 8.- Continued.

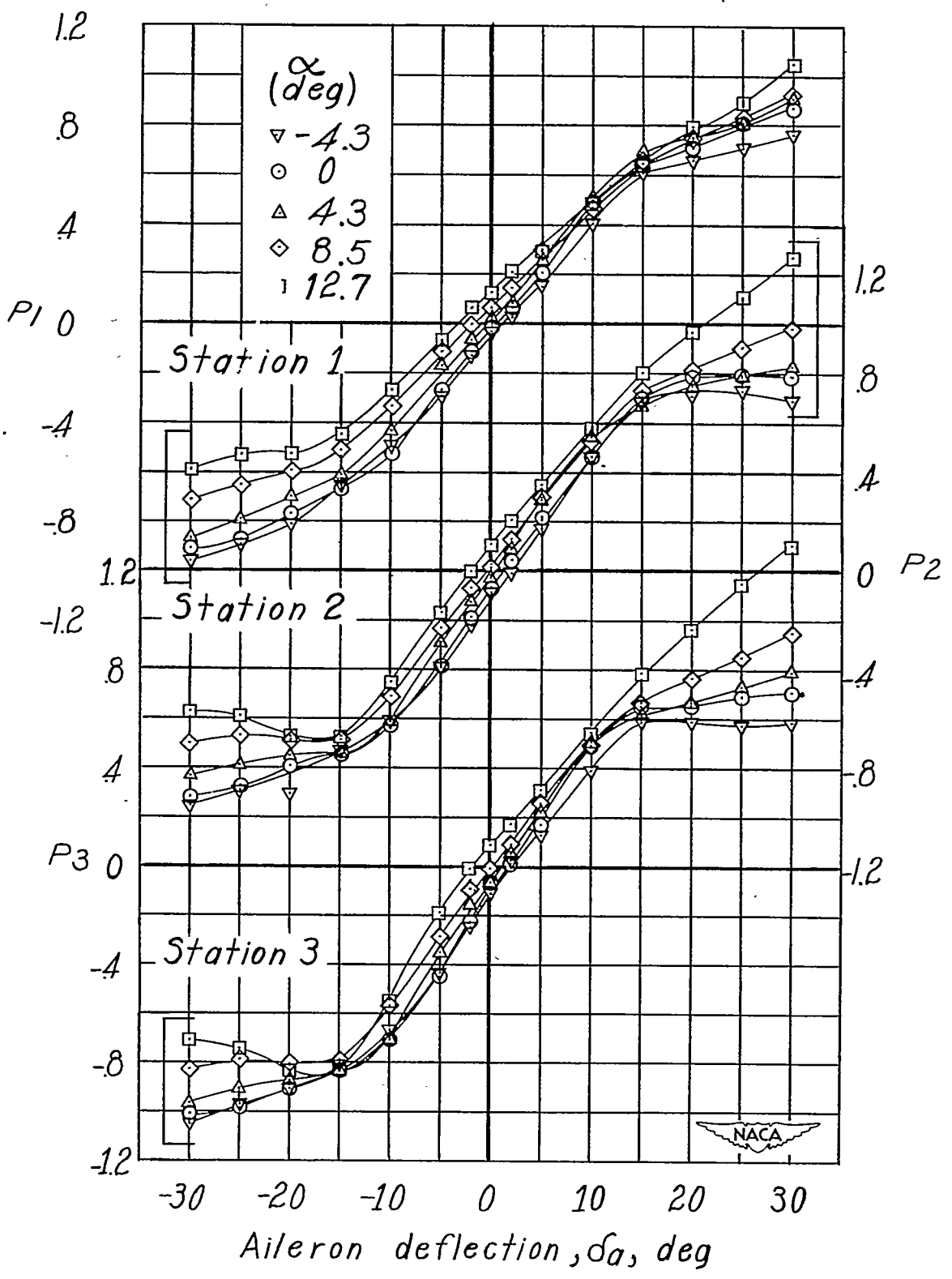

(c) Seal-pressure coefficient.

Figure 8.- Continued.

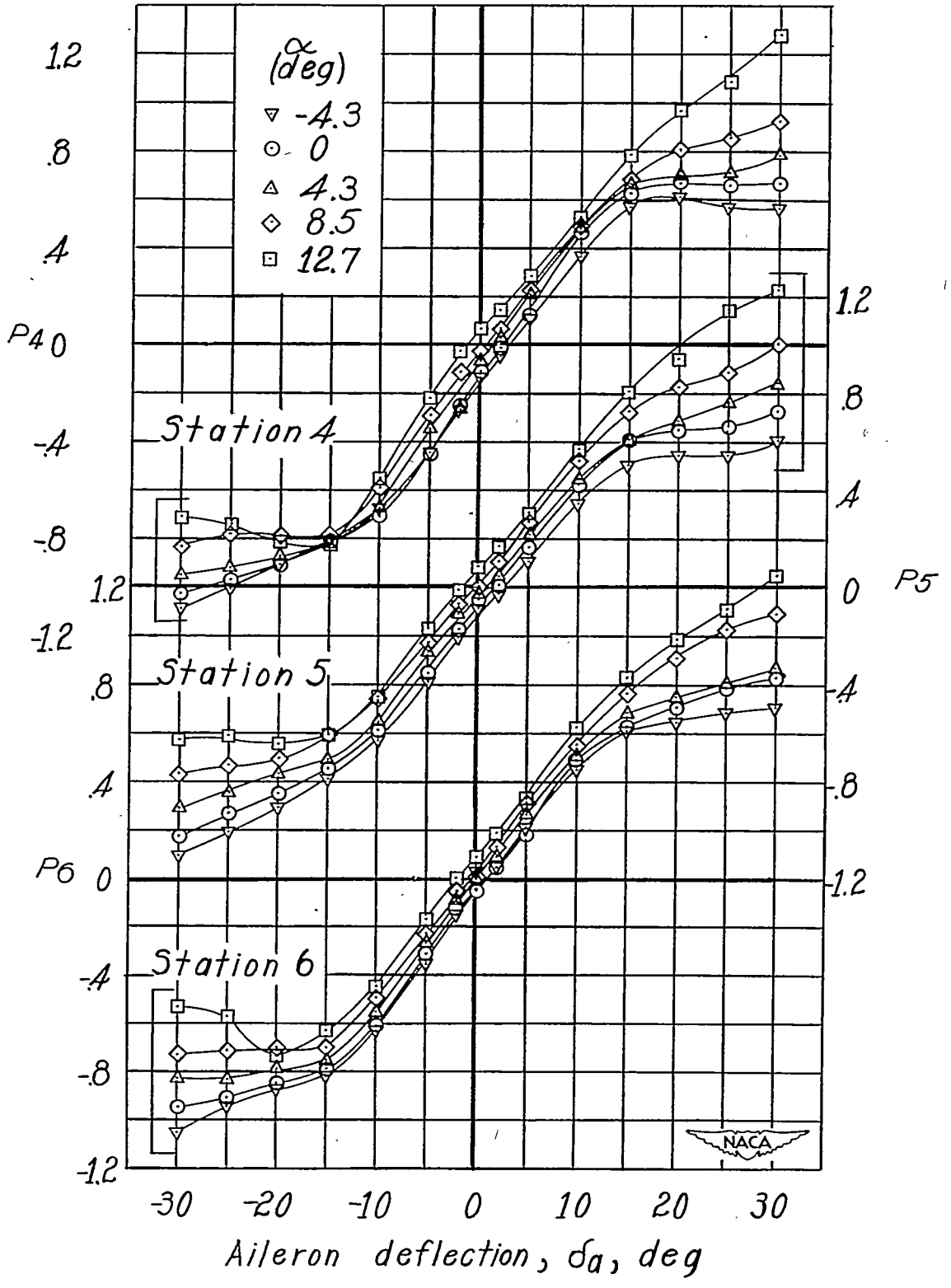

(c) Concluded.

Figure 8.- Concluded.

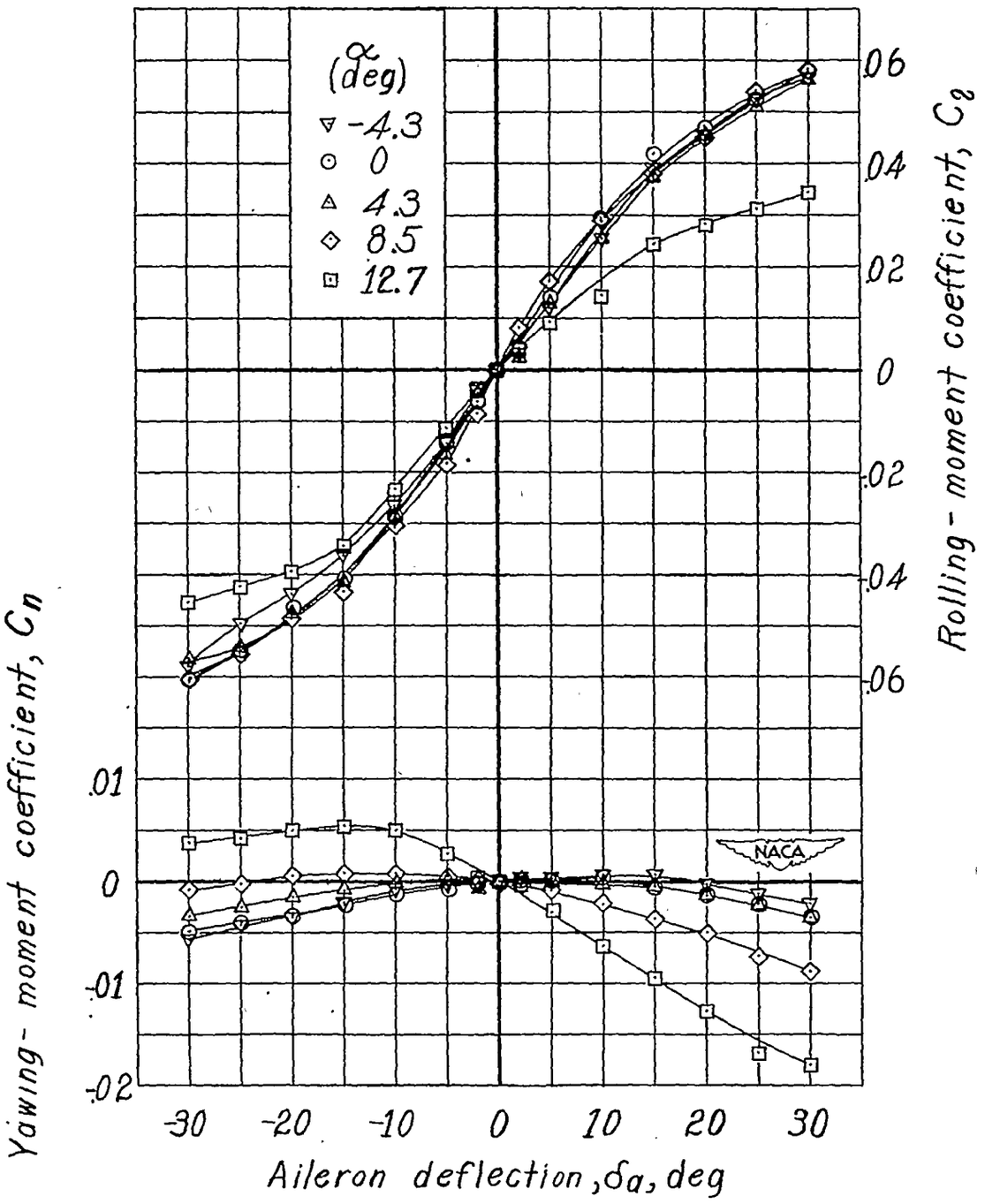

(a) Yawing- and rolling-moment coefficients.

Figure 9.- Variation of lateral control characteristics with aileron deflection. Aileron unsealed; $b_a = 0.95b_a'$; $\emptyset = 14^o$.

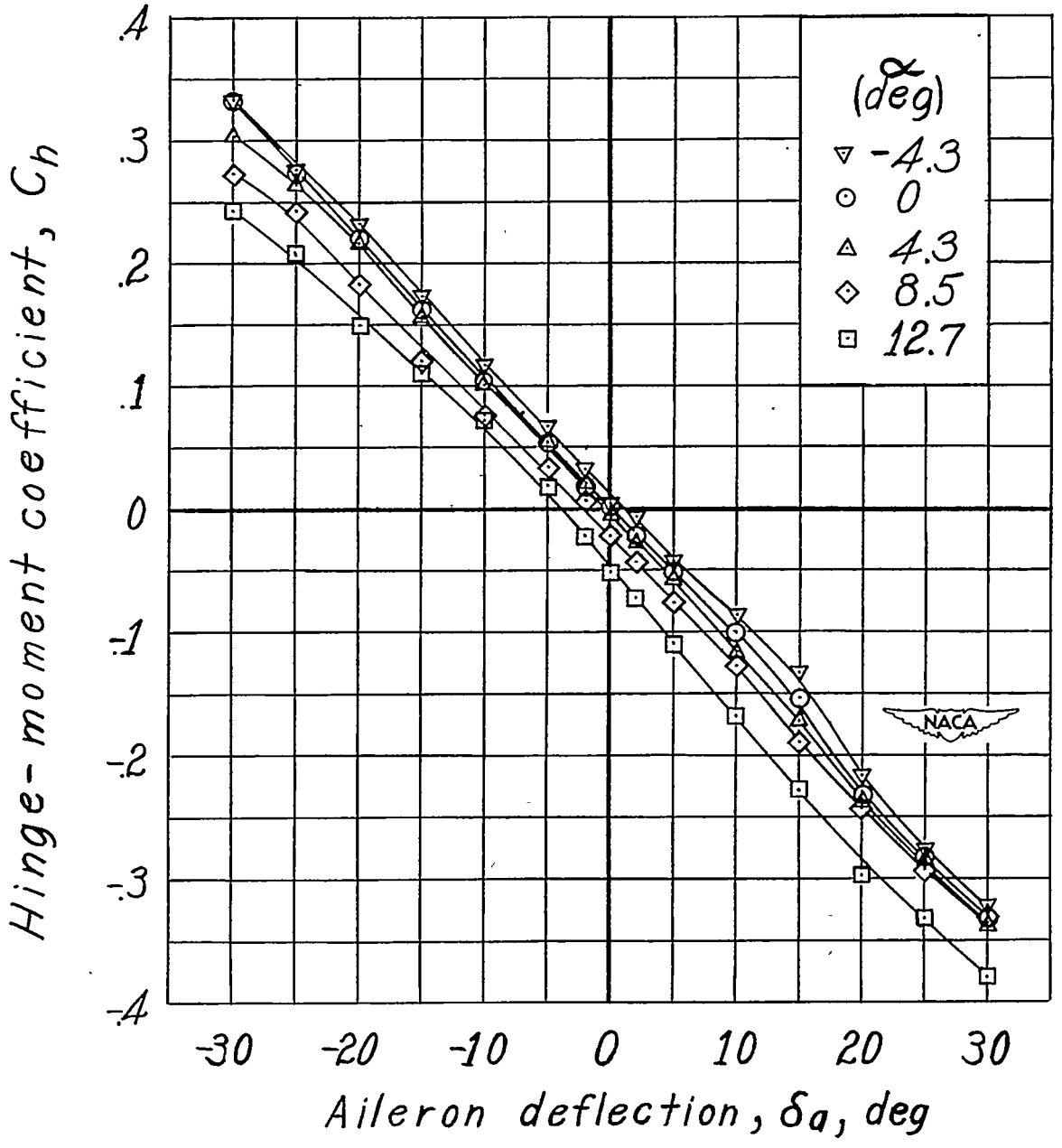

(b) Hinge-moment coefficient.

Figure 9.- Continued.

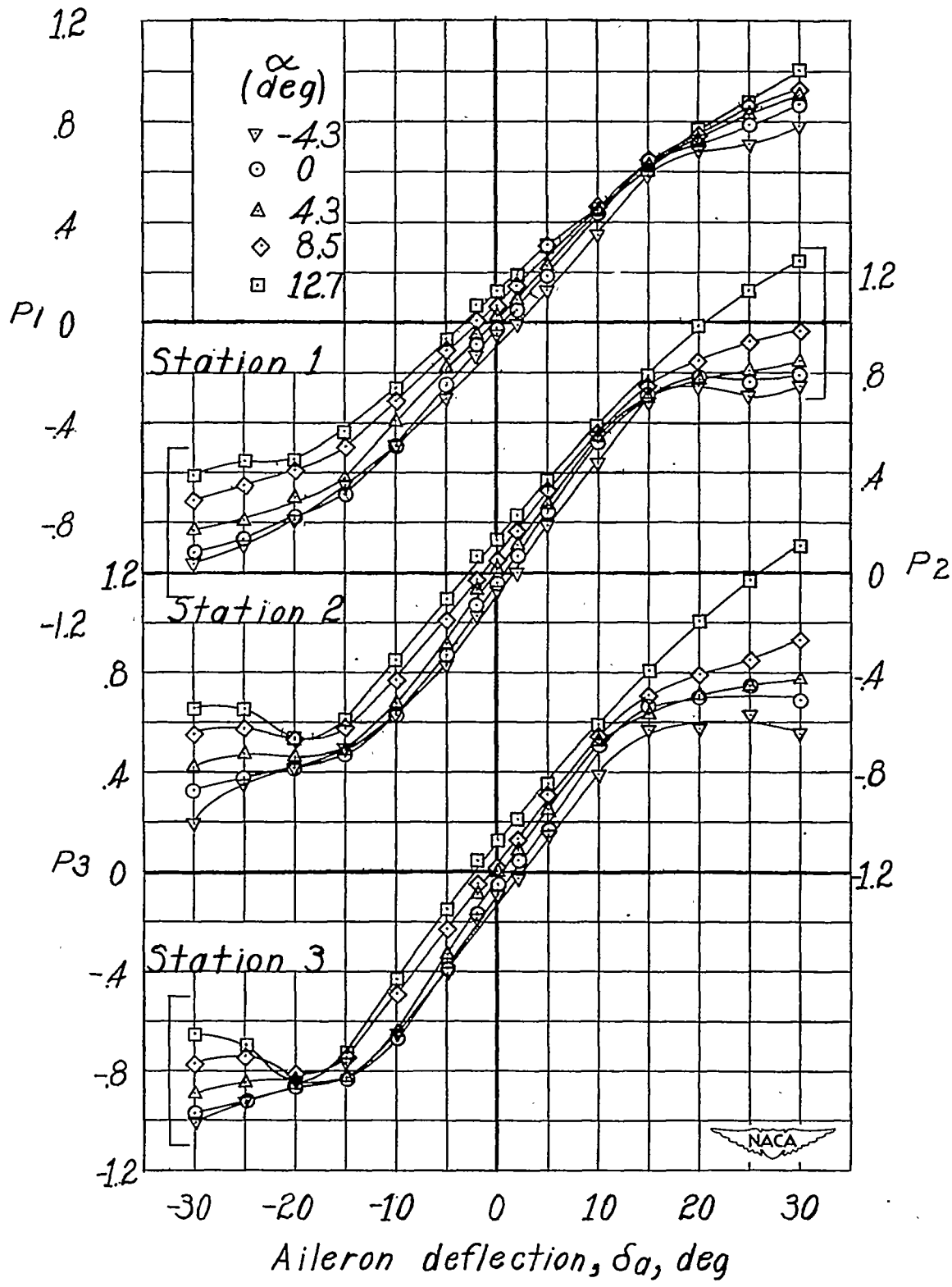

(c) Seal-pressure coefficient.

Figure 9.- Continued.

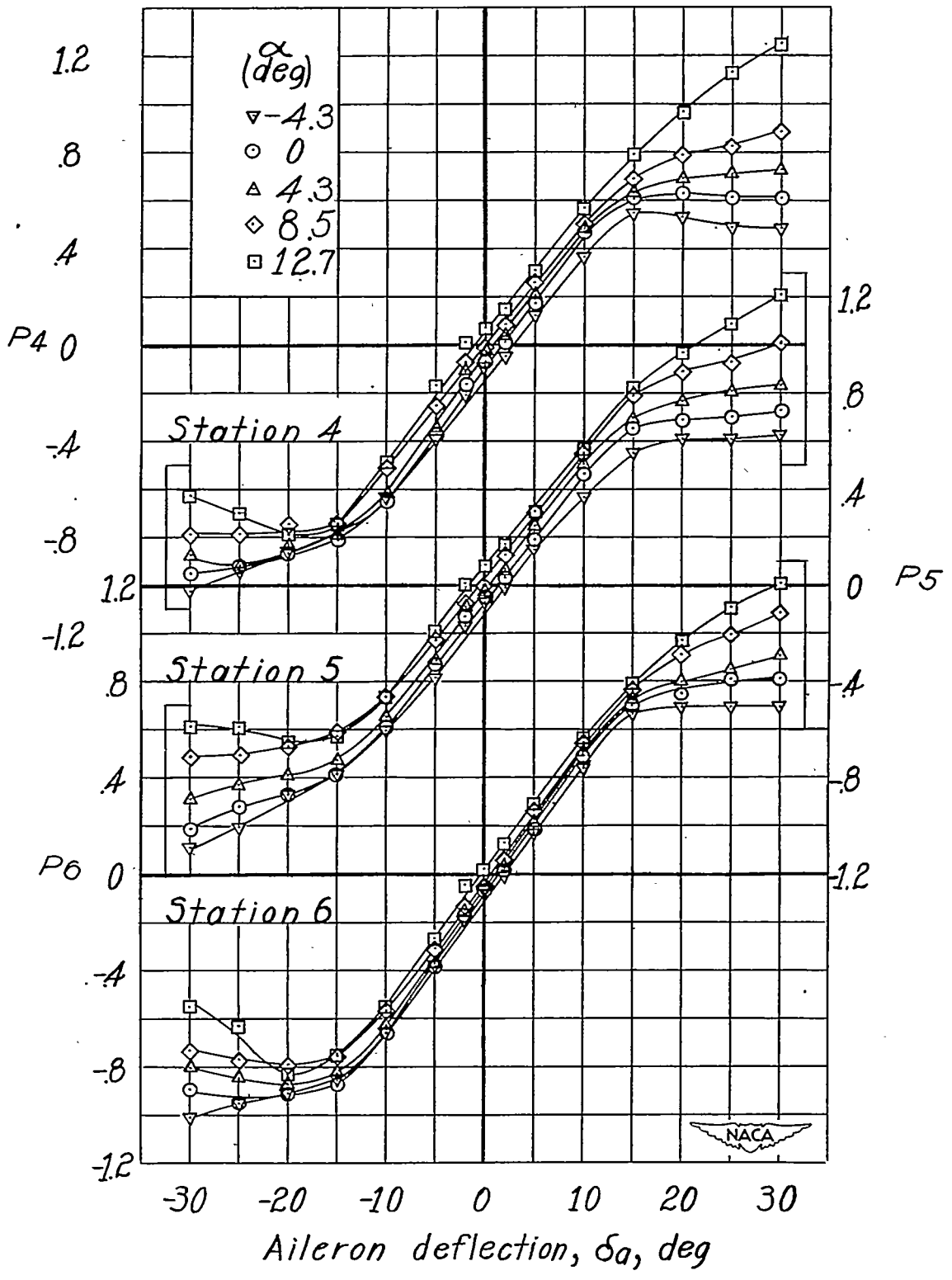

(c) Concluded.

Figure 9.- Concluded.

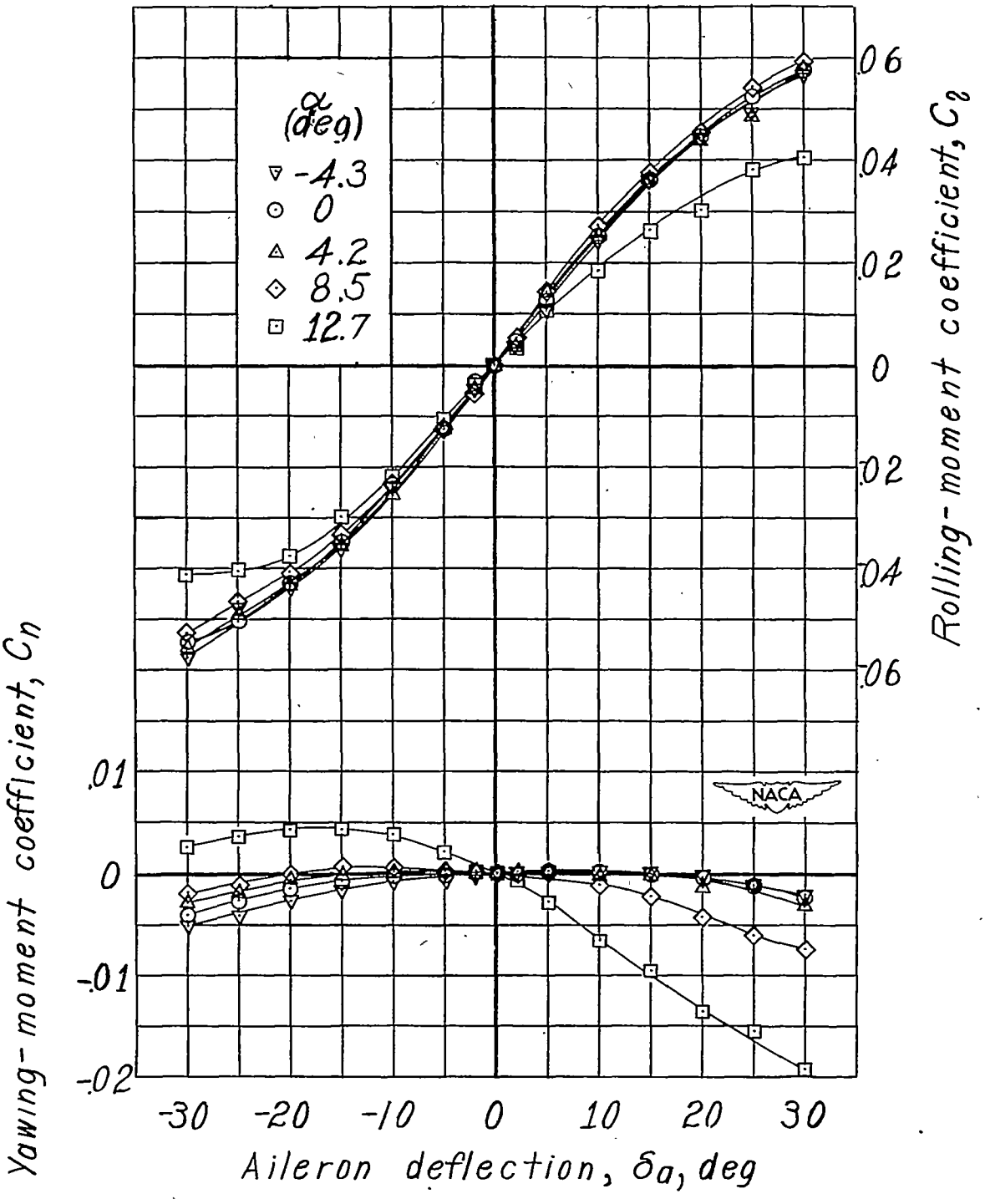

(a) Yawing- and rolling-moment coefficients.

Figure 10.- Variation of lateral control characteristics with aileron deflection. Aileron sealed; $b_a = 0.95b_a'$; $\emptyset = 25^o$.

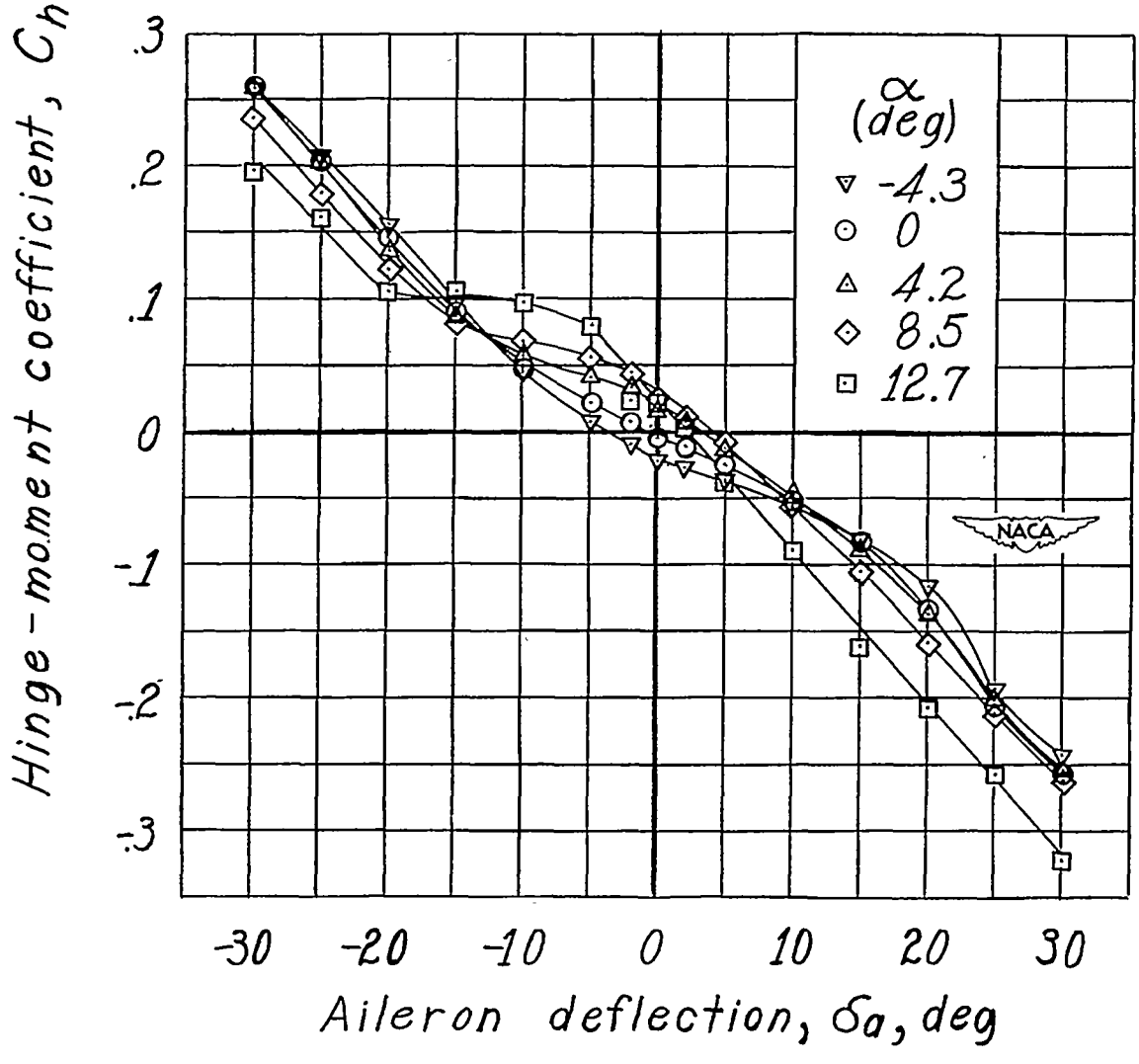

(b) Hinge-moment coefficient.

Figure 10.- Continued.

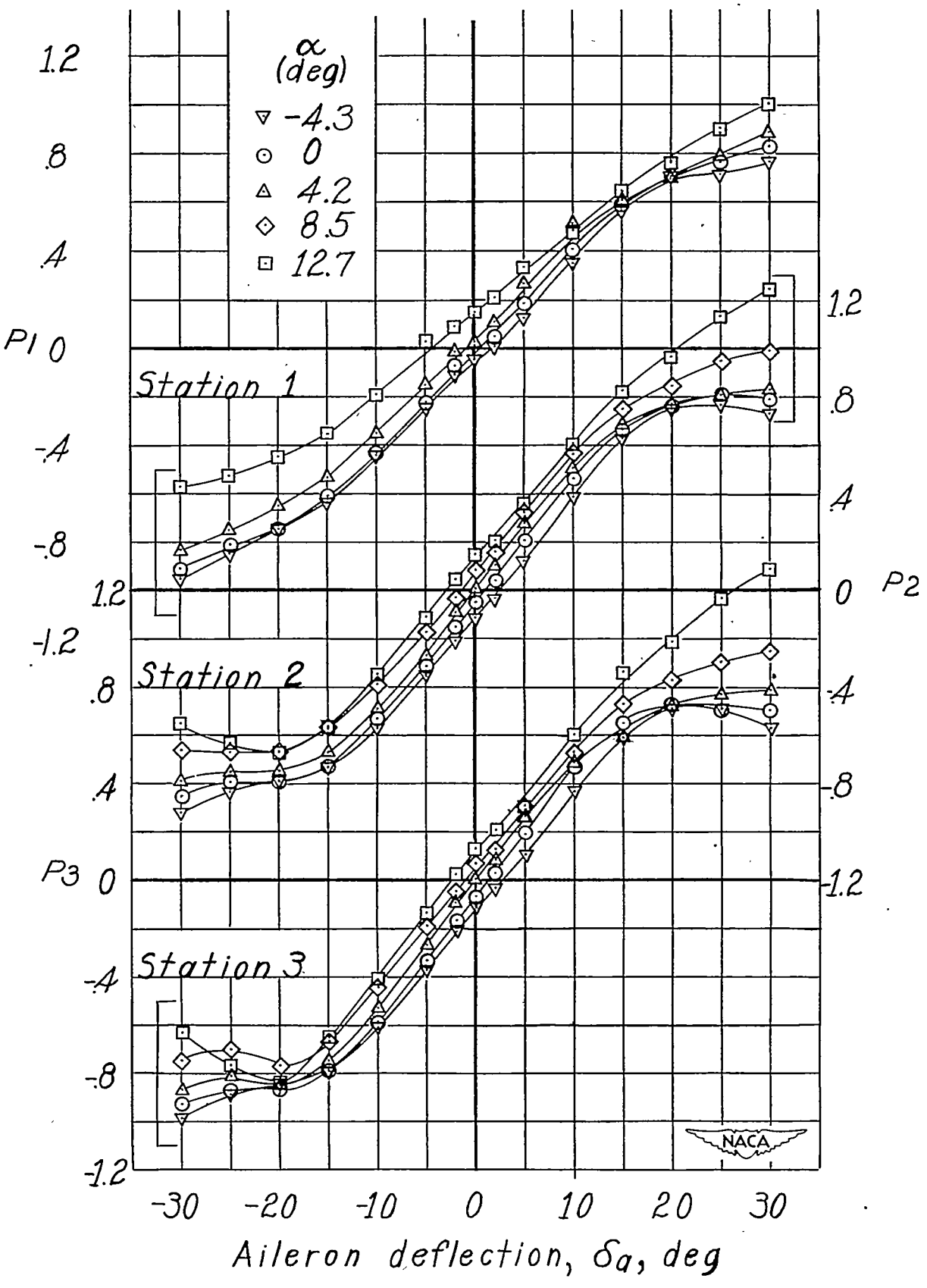

(c) Seal-pressure coefficient.

Figure 10.- Continued.

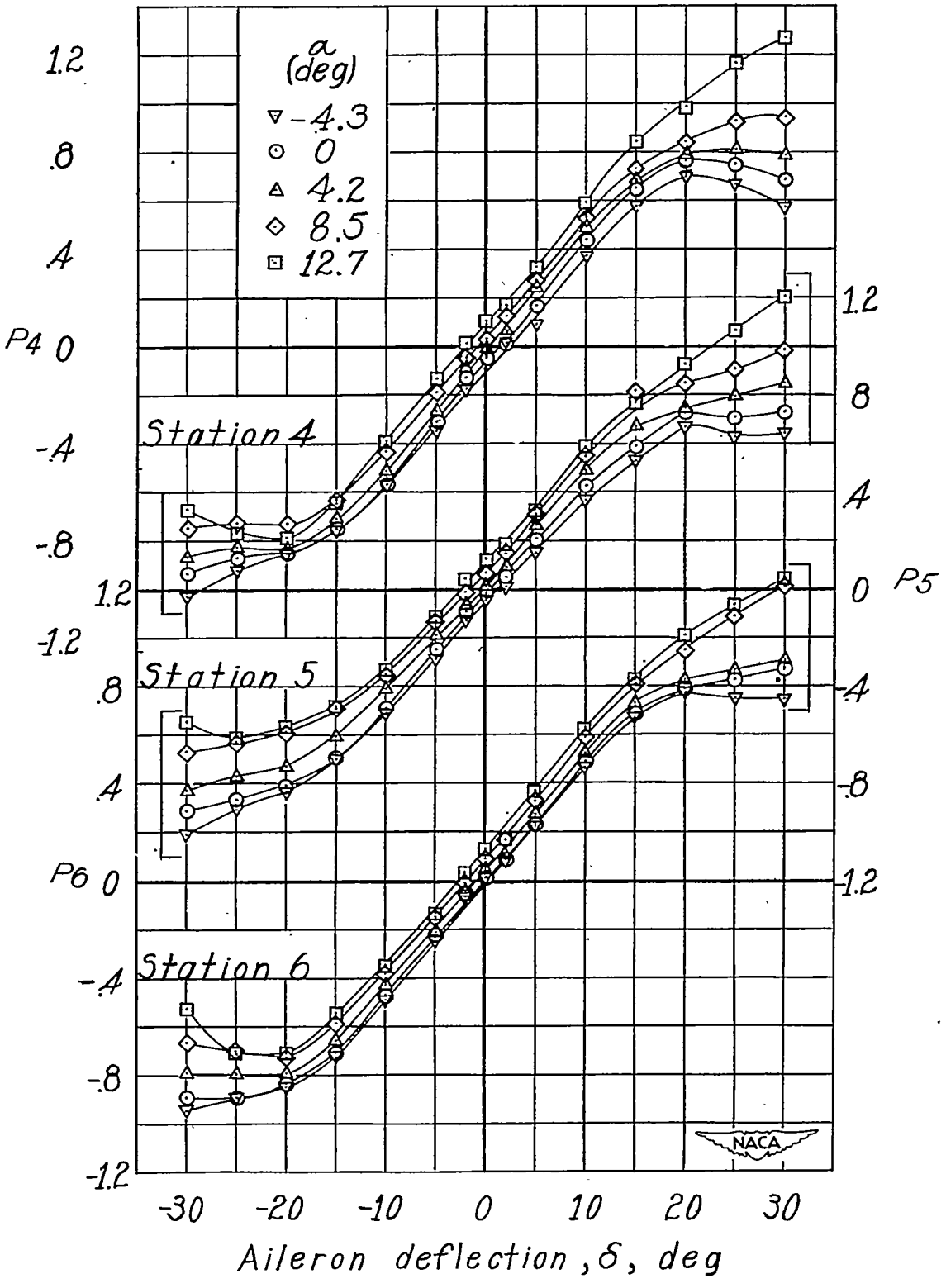

(c) Concluded.

Figure 10.- Concluded.

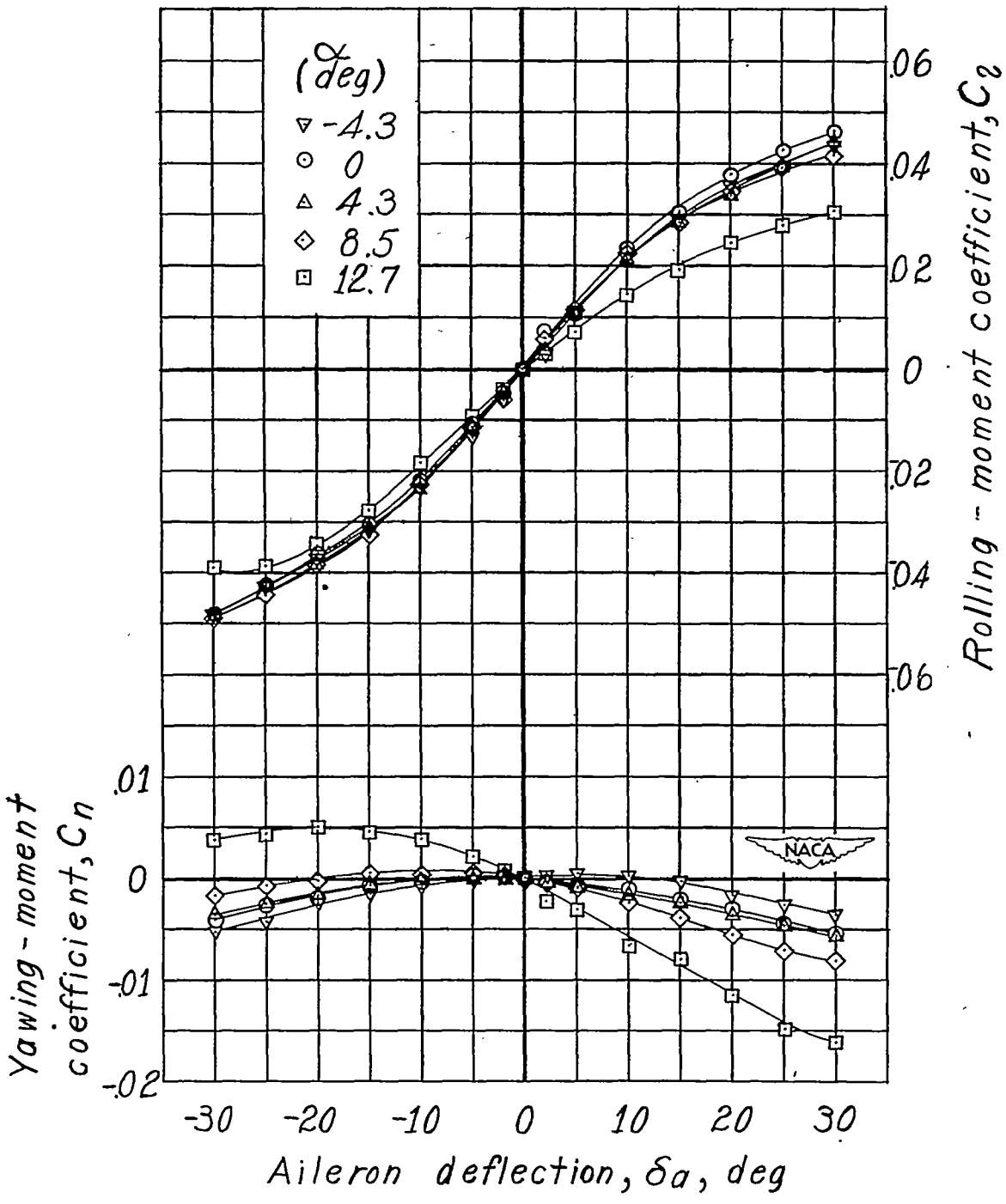

(a) Yawing- and rolling-moment coefficients.

Figure 11.- Variation of lateral control characteristics with aileron deflection. Aileron sealed; $b_a = 0.58b_a'$; $\emptyset = 6^o$.

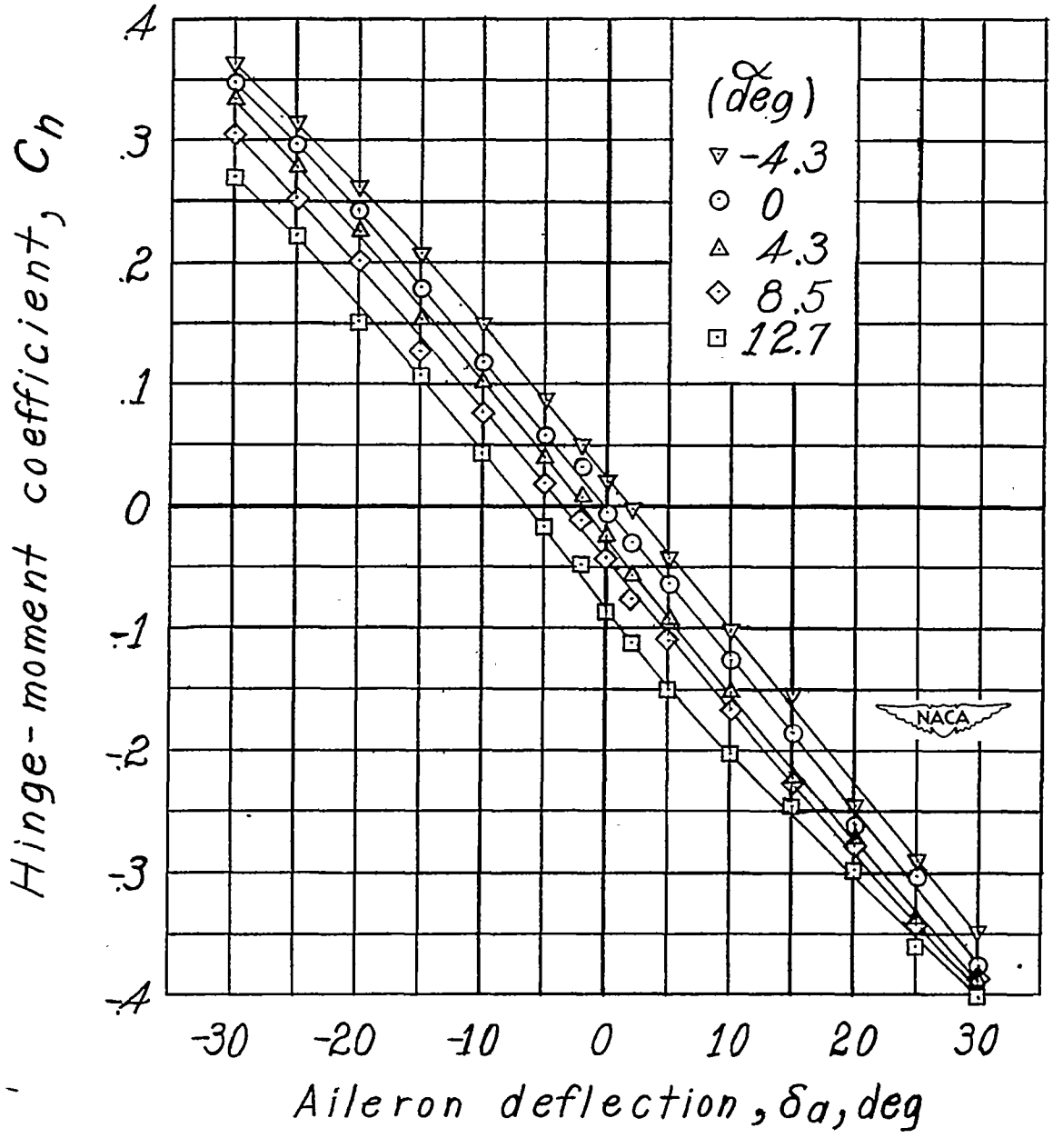

(b) Hinge-moment coefficient.

Figure 11.- Continued.

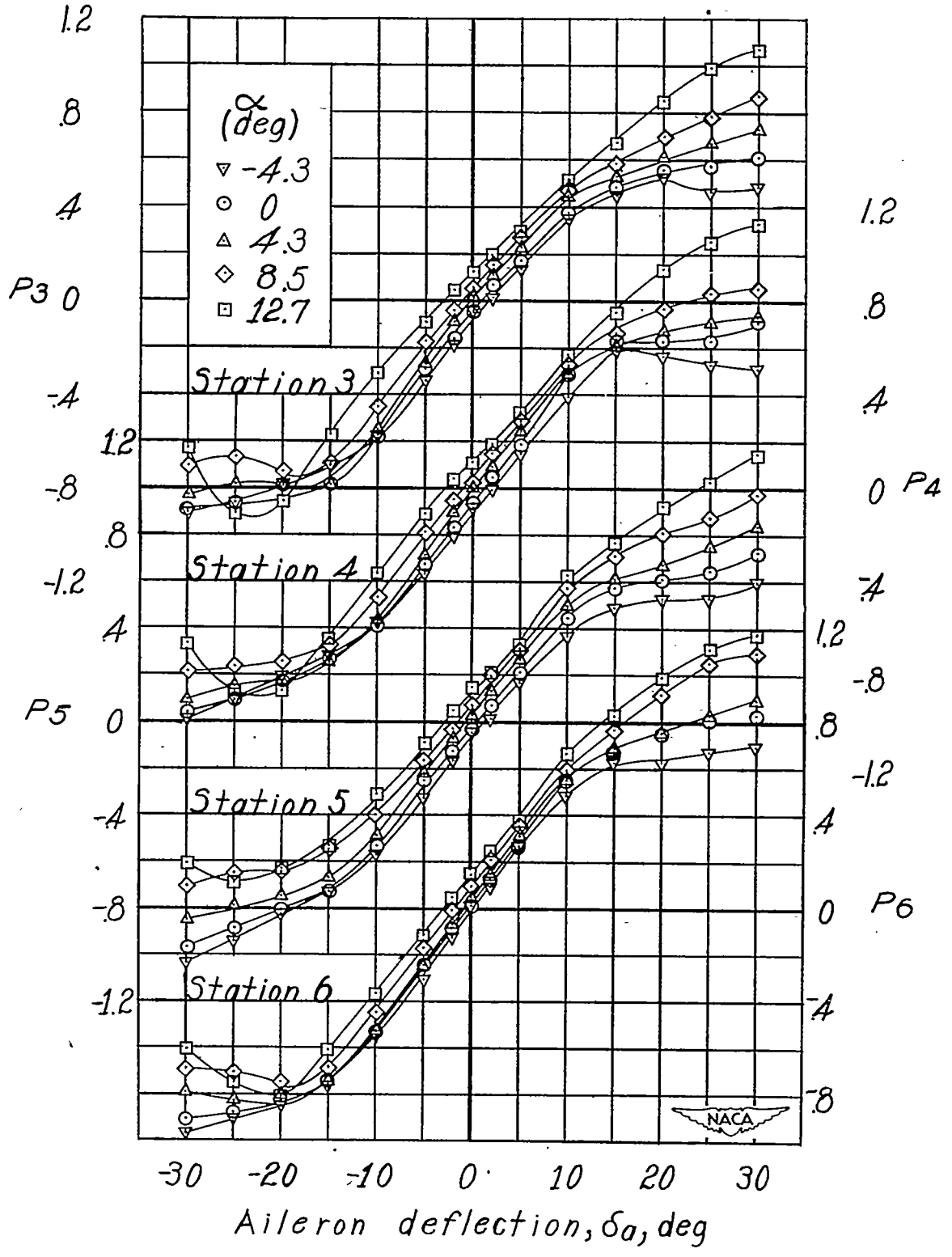

(c) Seal-pressure coefficeint..

Figure 11.- Concluded.

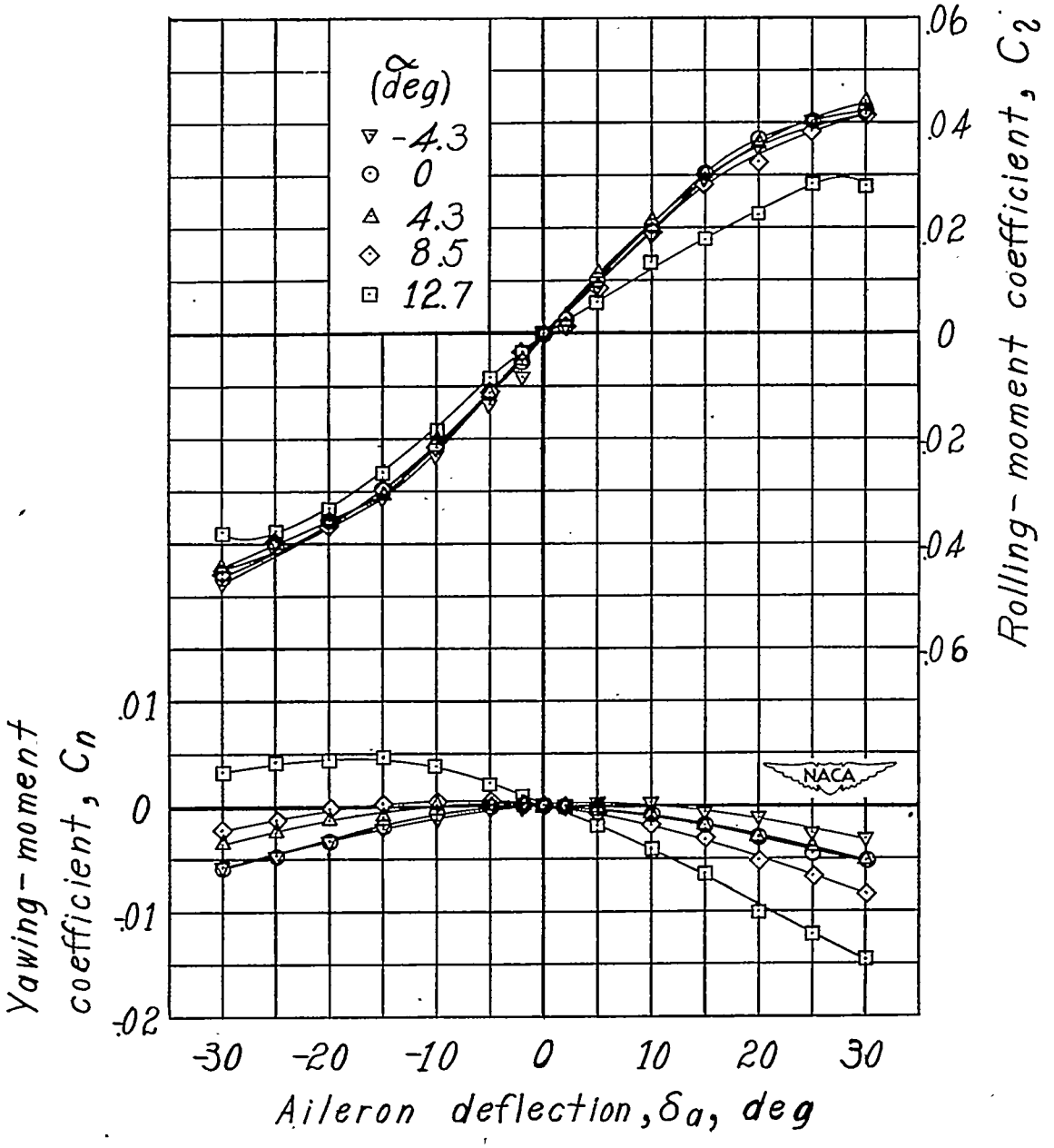

(a) Yawing- and rolling-moment coefficients.

Figure 12.- Variation of lateral control characteristics with aileron deflection. Aileron sealed; $b_a = 0.58b_a'$; $\emptyset = 14^o$.

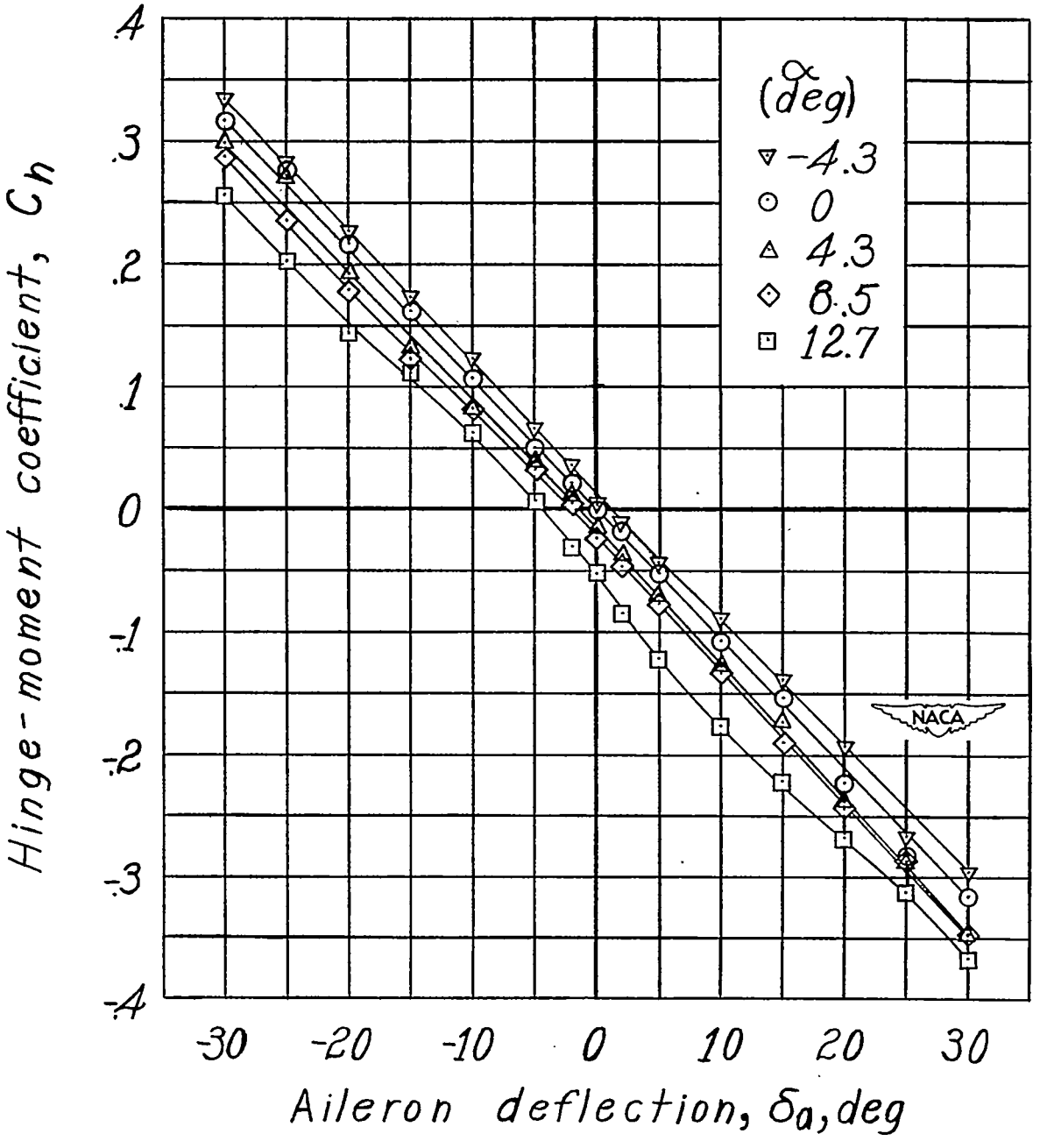

(b) Hinge-moment coefficient.

Figure 12.- Continued.

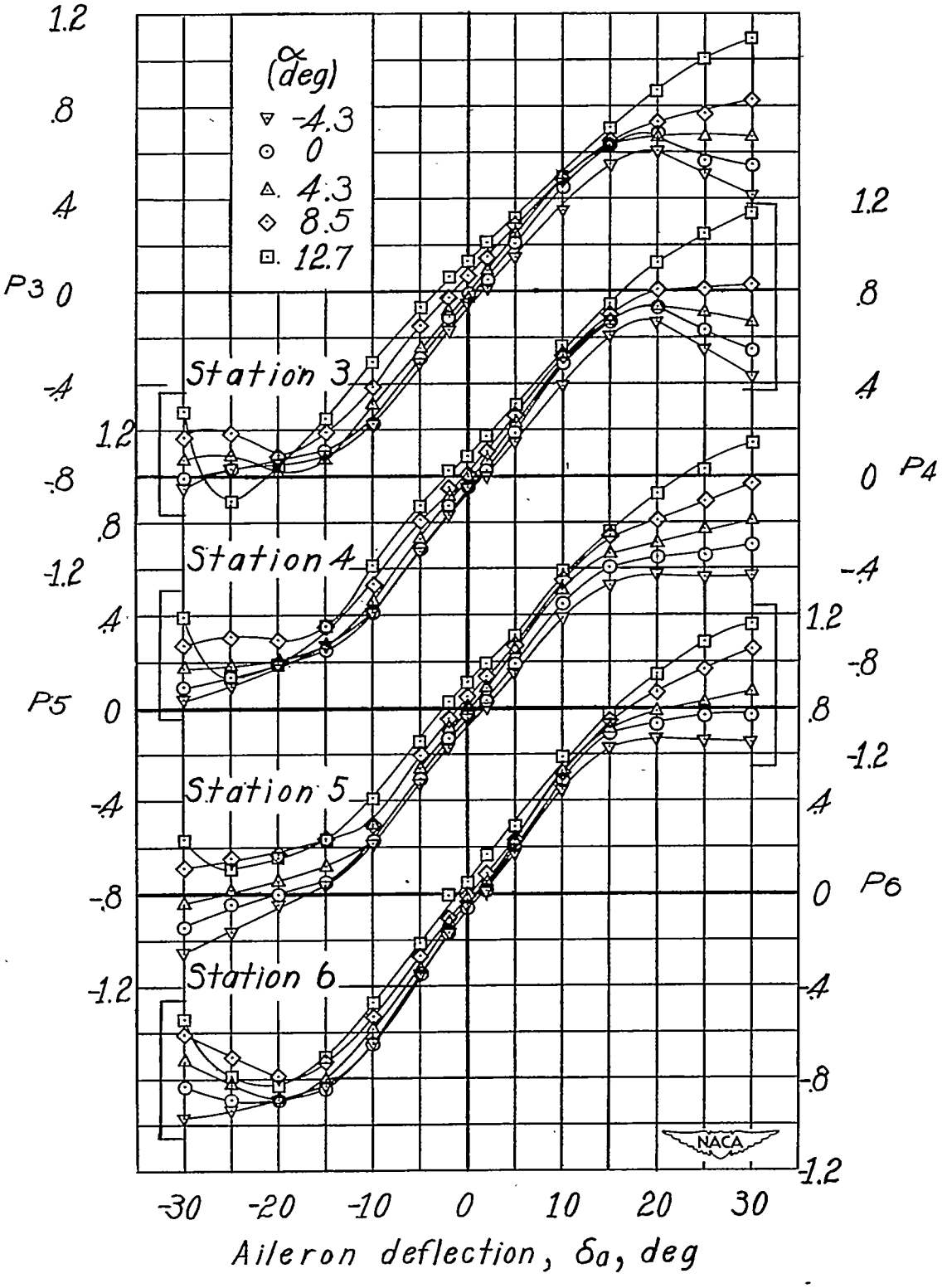

(c) Seal-pressure coefficient.

Figure 12.- Concluded.

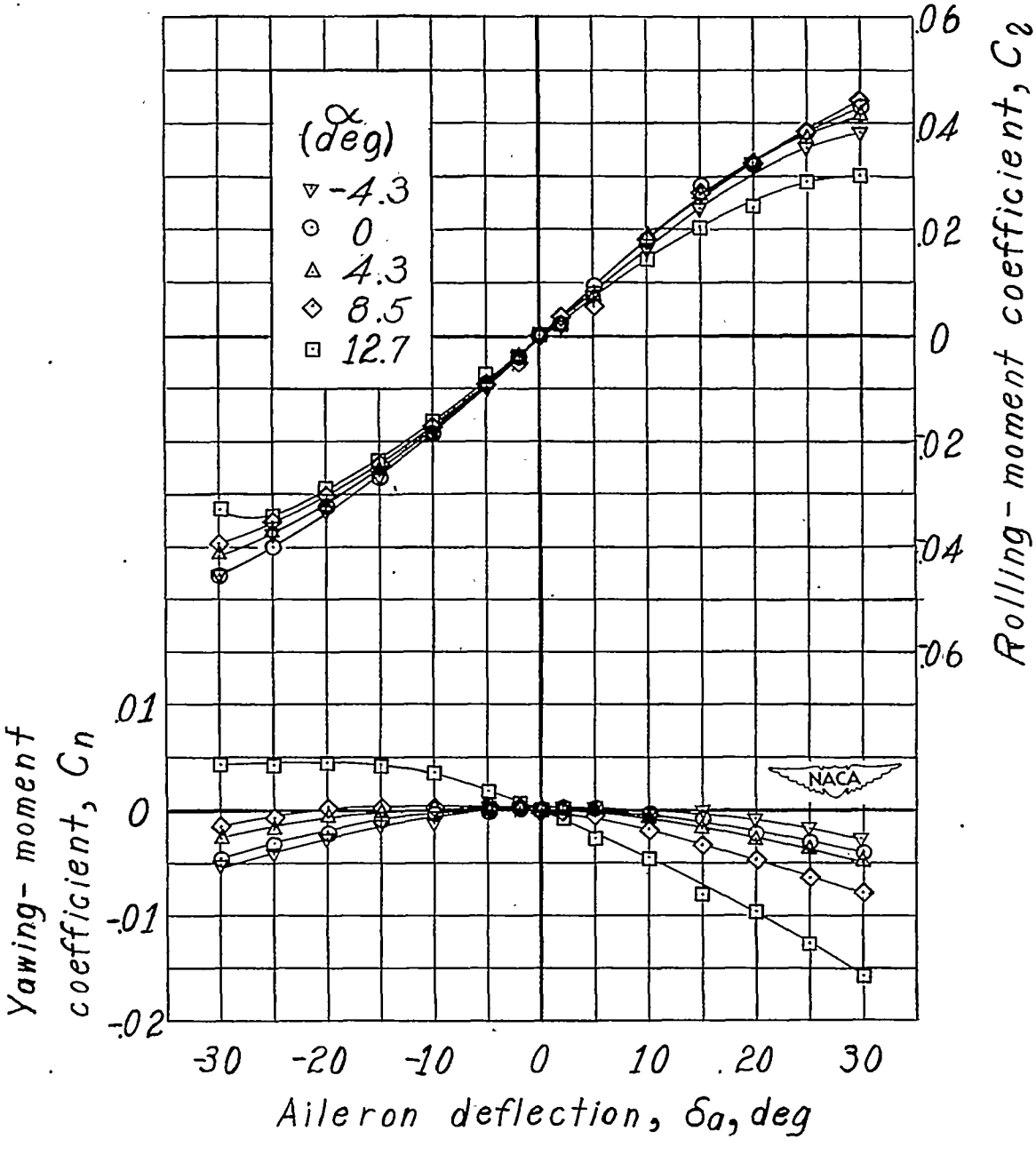

(a) Yawing- and rolling-moment coefficients.

Figure 13.- Variation of lateral control characteristics with aileron deflection. Aileron sealed; $b_a = 0.58b_a'$; $\emptyset = 25^\circ$.

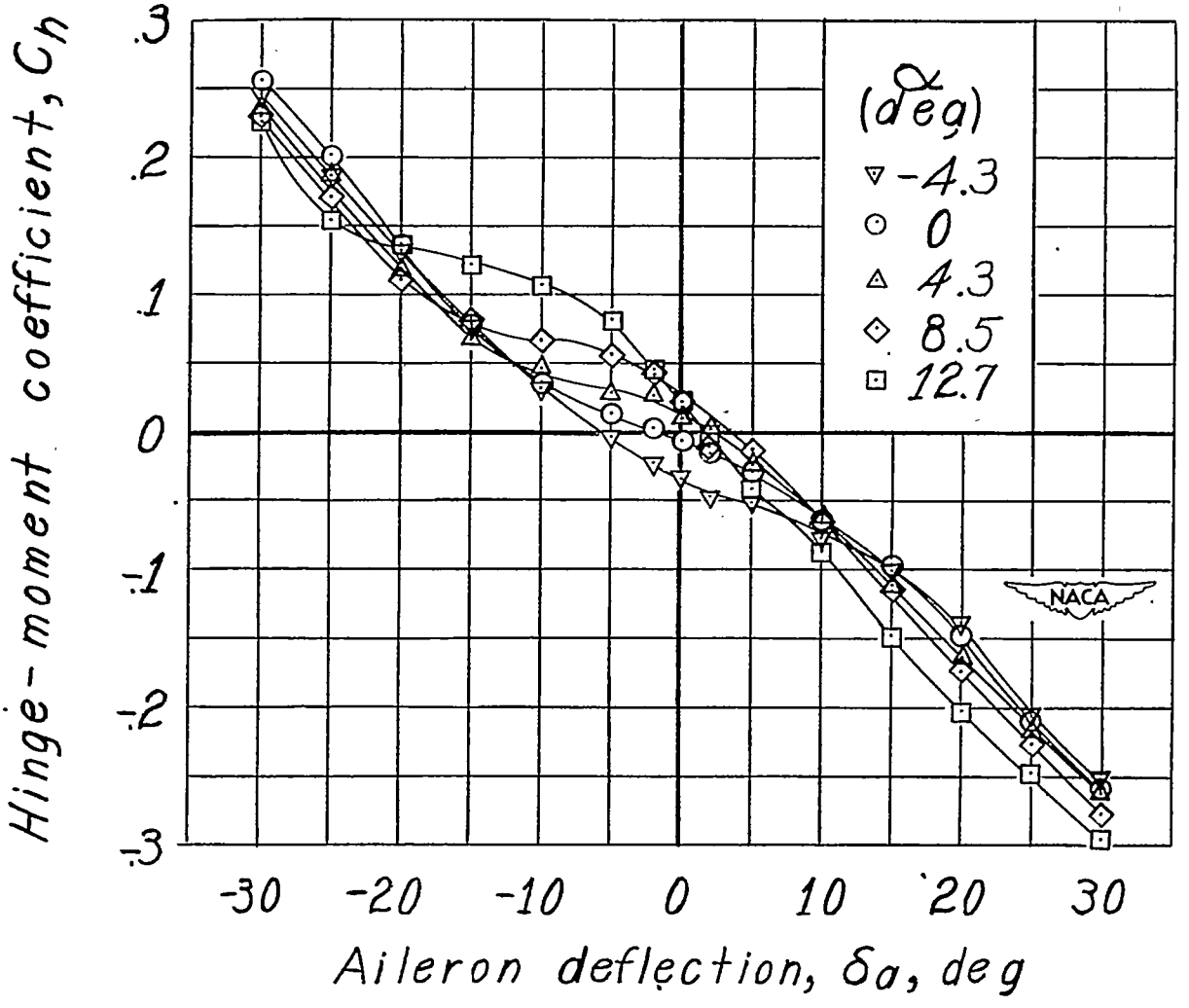

(b) Hinge-moment coefficient.

Figure 13.- Continued.

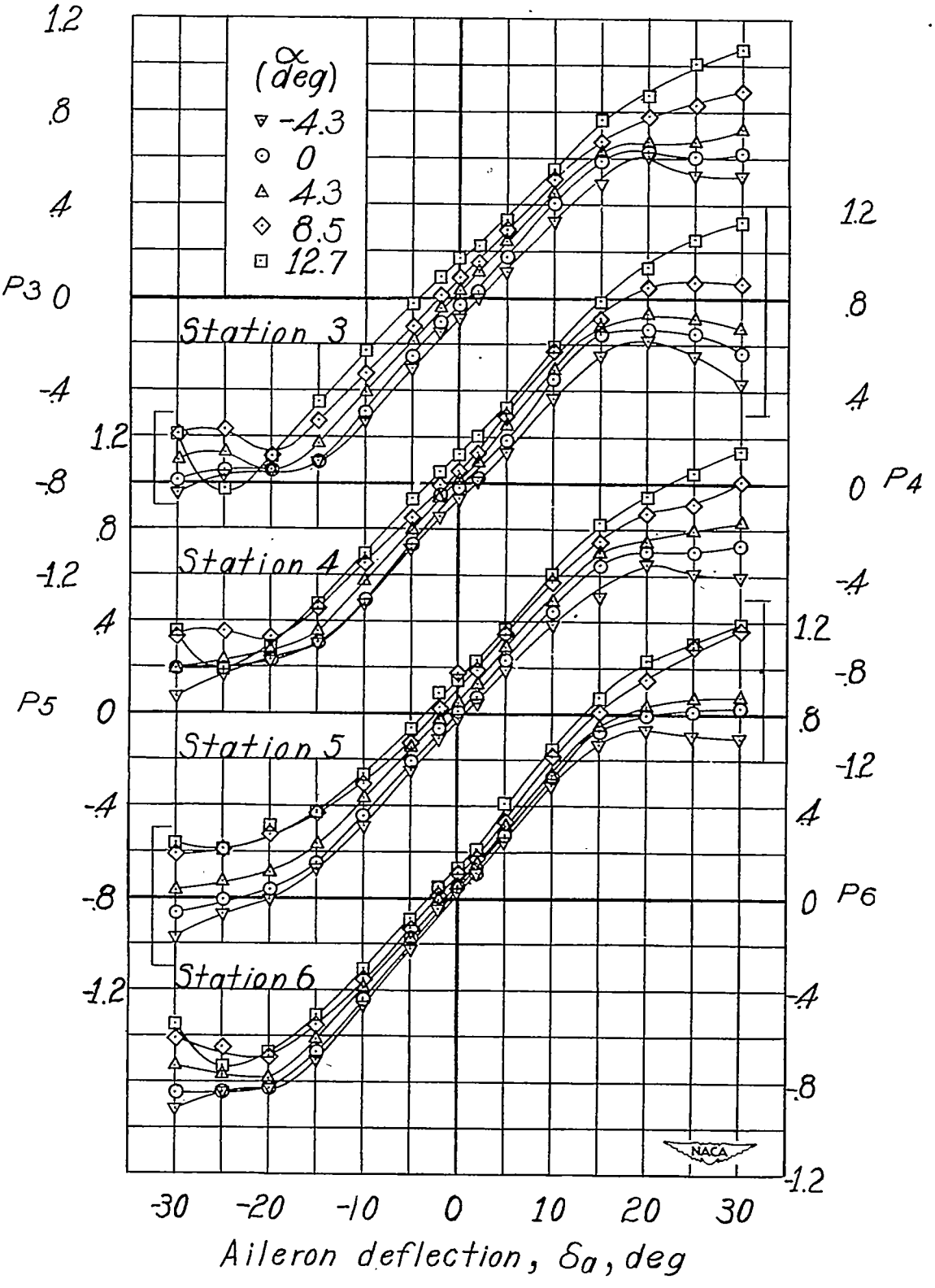

(c) Seal-pressure coefficient.

Figure 13.- Concluded.

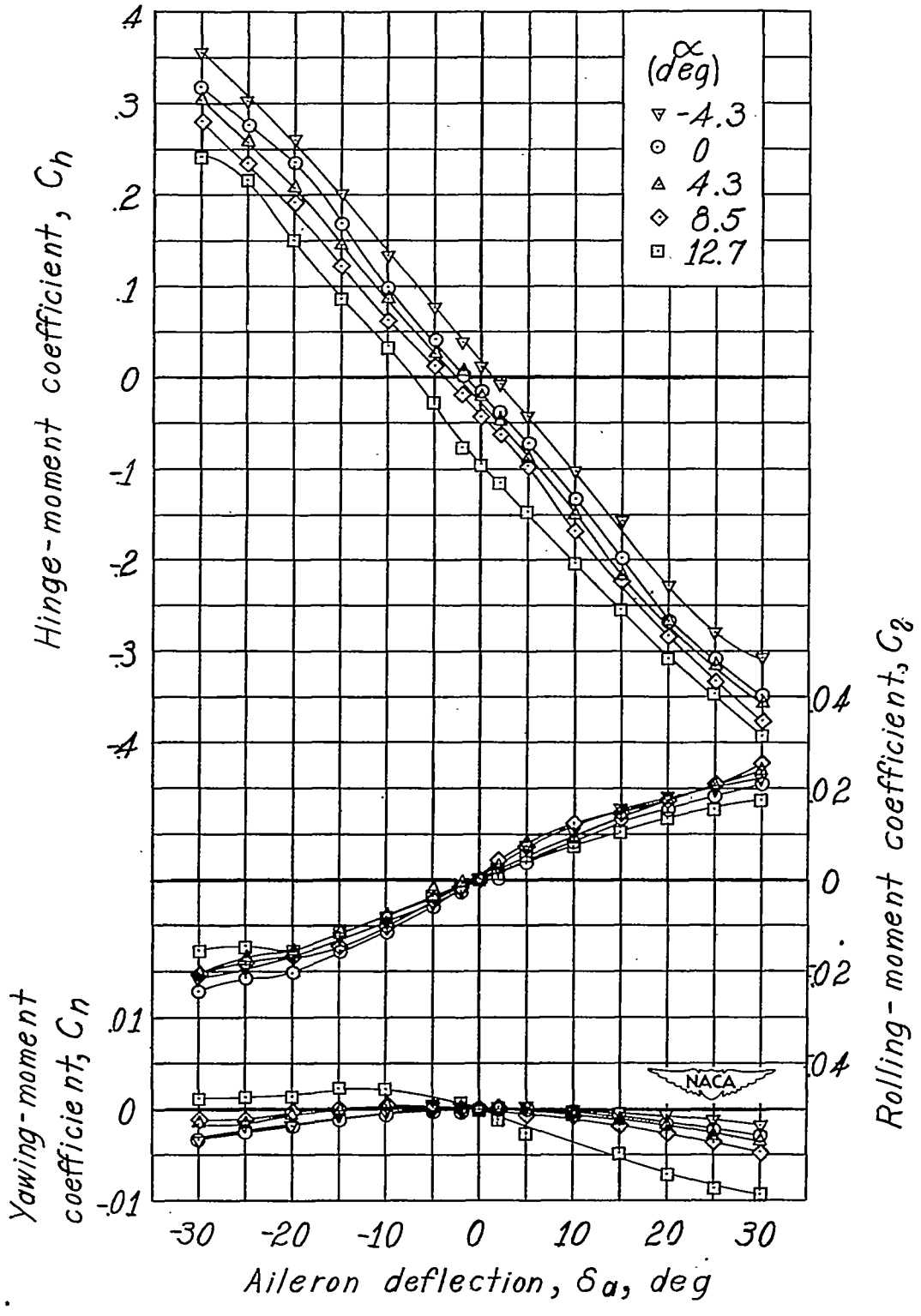

(a) Yawing-, rolling-, and hinge-moment coefficients.

Figure 14.- Variation of lateral control characteristics with aileron deflection. Aileron sealed; $b_a = 0.29b_a'$; $\phi = 6^\circ$.

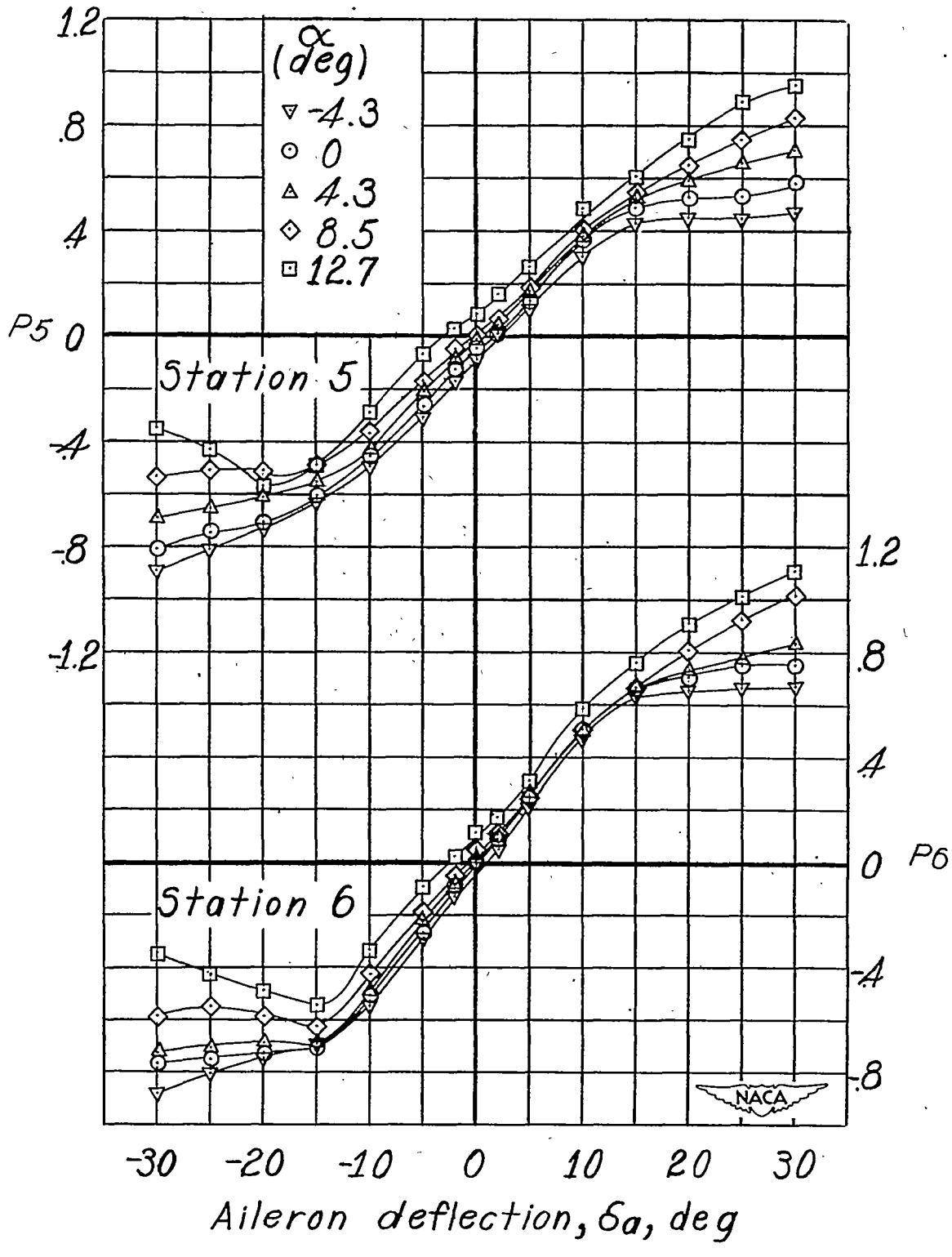

(b) Seal-pressure coefficient.

Figure 14.- Concluded.

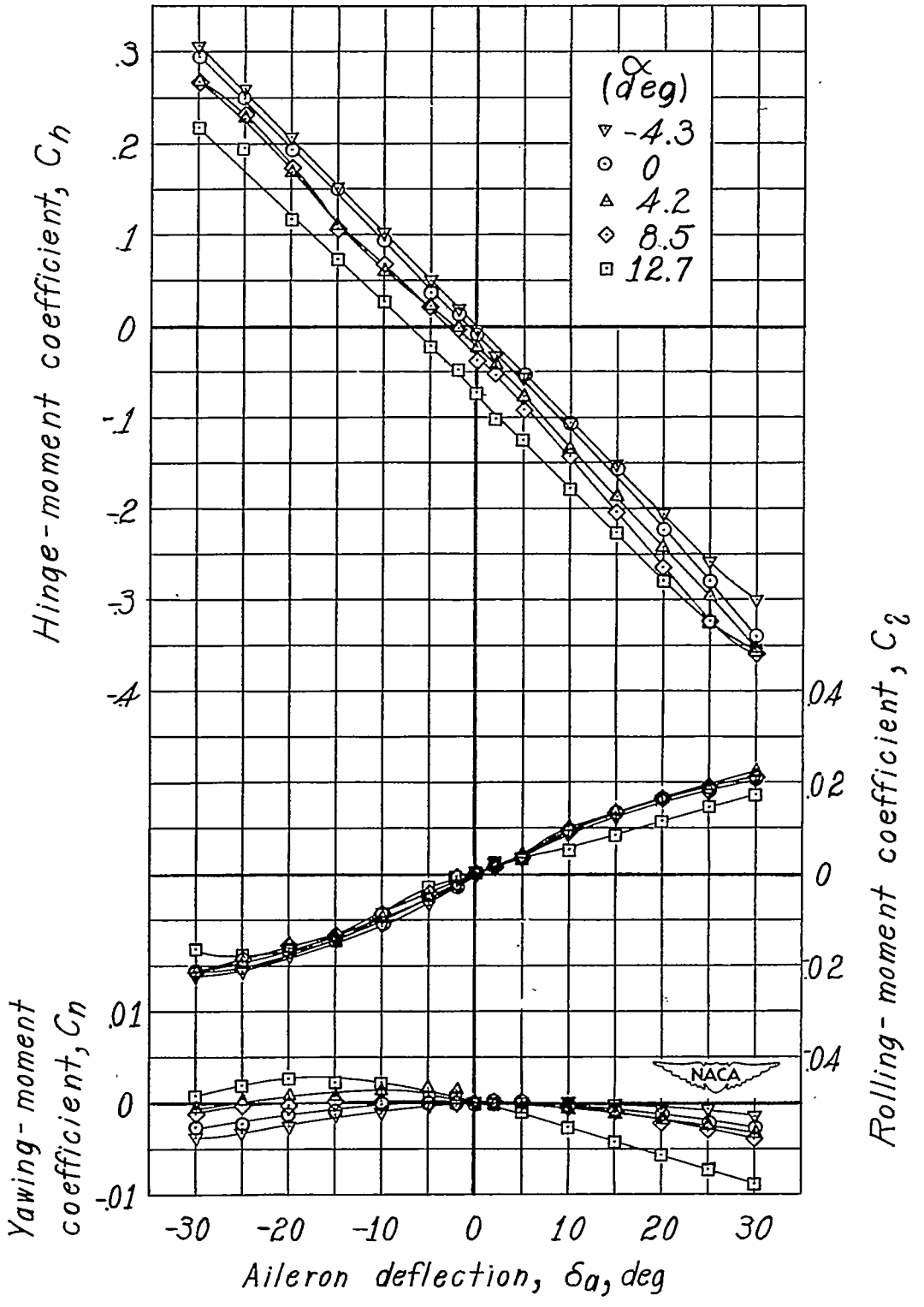

(a) Yawing-, rolling-, and hinge-moment coefficients.

Figure 15.- Variation of lateral control characteristics with aileron deflection. Aileron sealed; $b_a = 0.29b_a'$; $\phi = 14^\circ$.

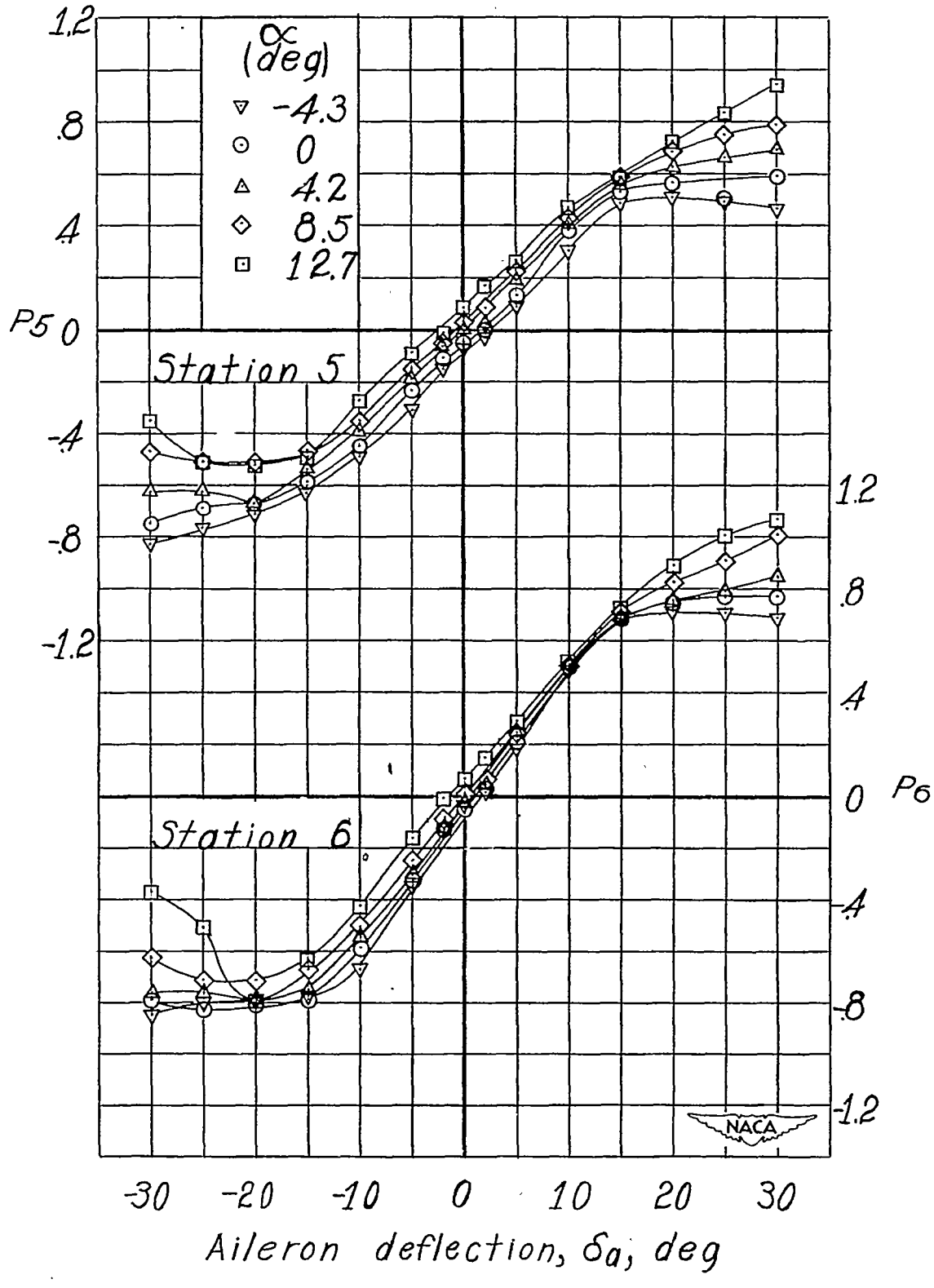

(b) Seal-pressure coefficient.

Figure 15.- Concluded.

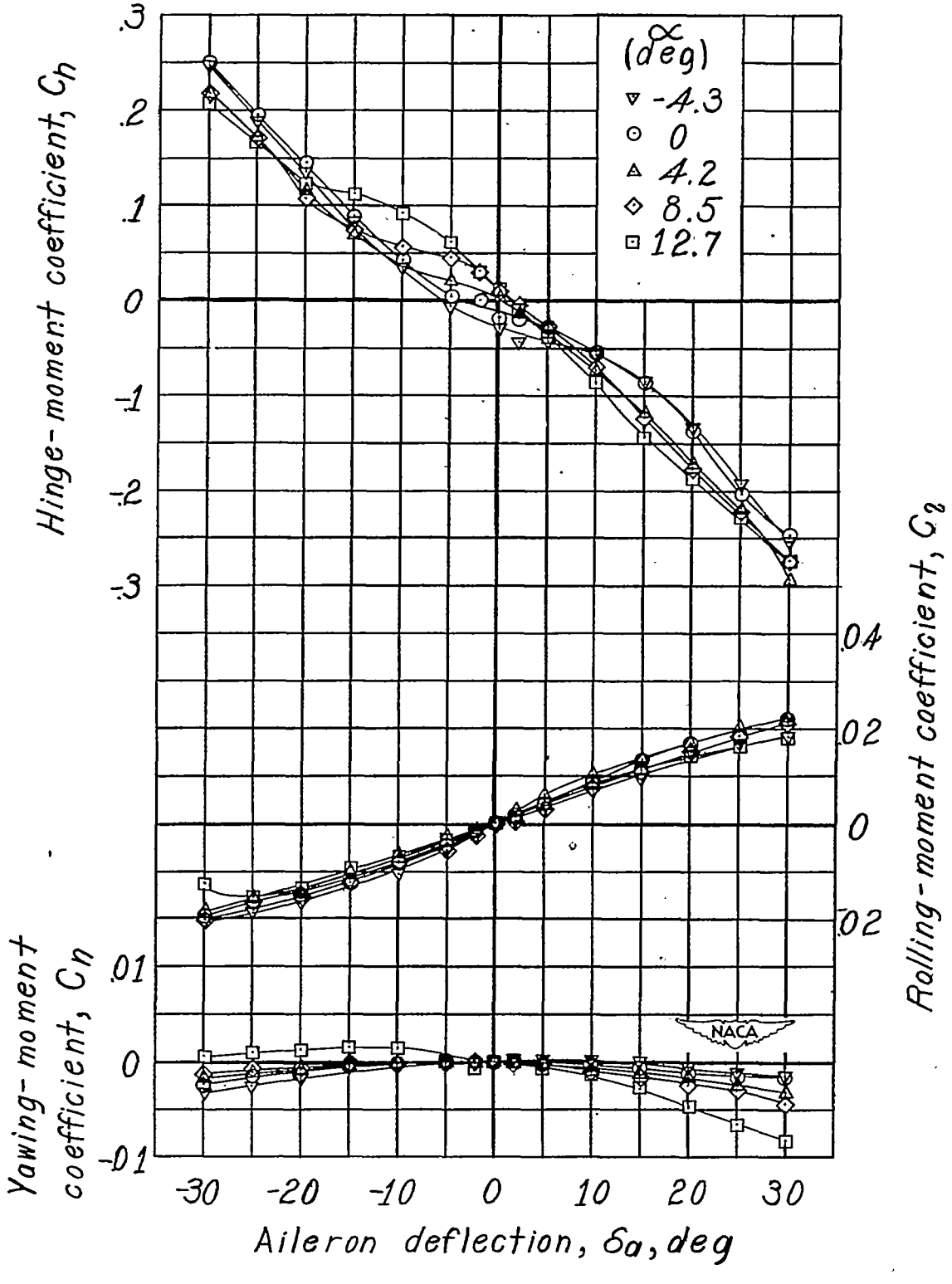

(a) Yawing-, rolling-, and hinge-moment coefficients.

Figure 16.- Variation of lateral control characteristics with aileron deflection. Aileron sealed; $b_a = 0.29b_a'$; $\phi = 25^\circ$.

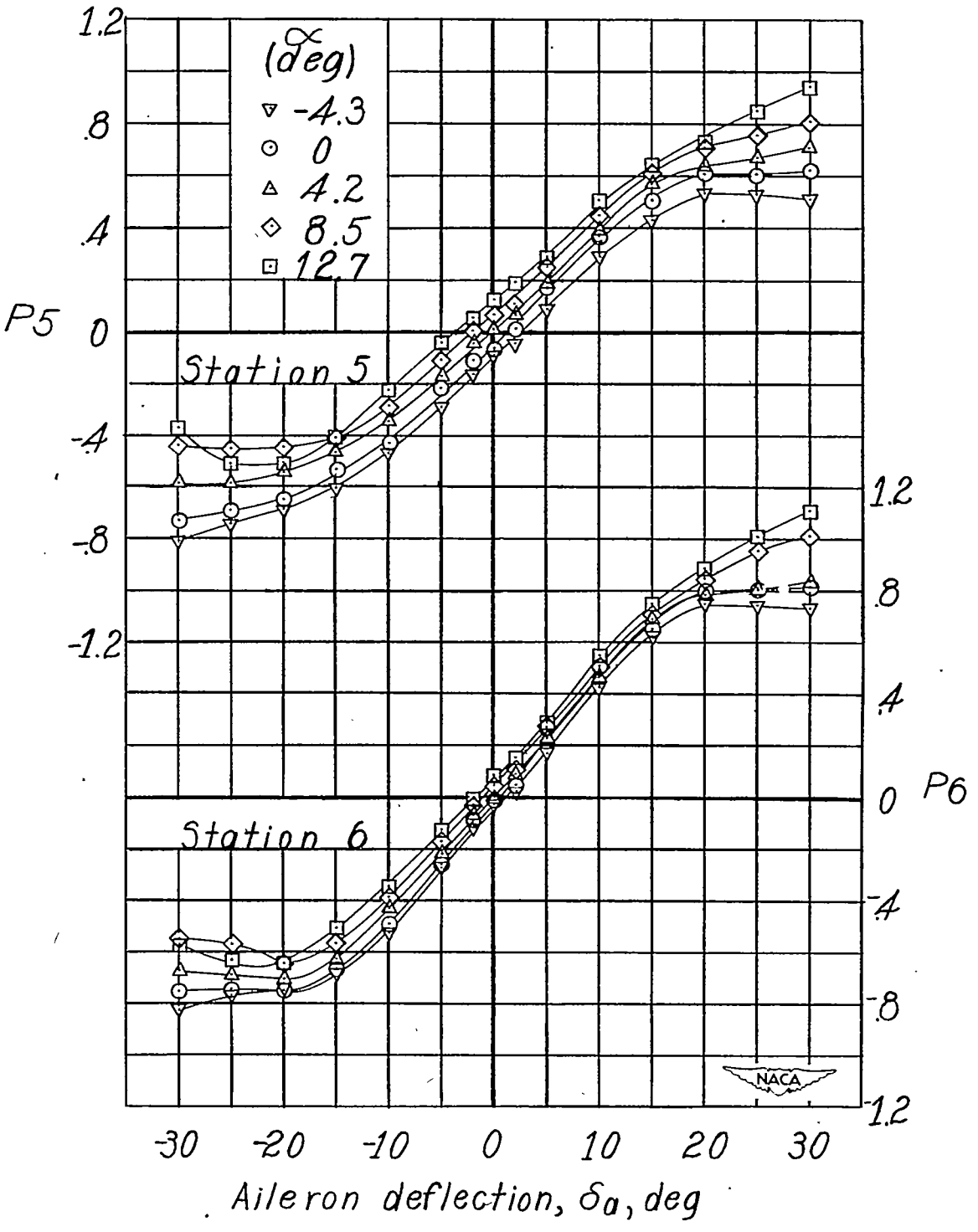

(b) Seal-pressure coefficient.

Figure 16.- Concluded.

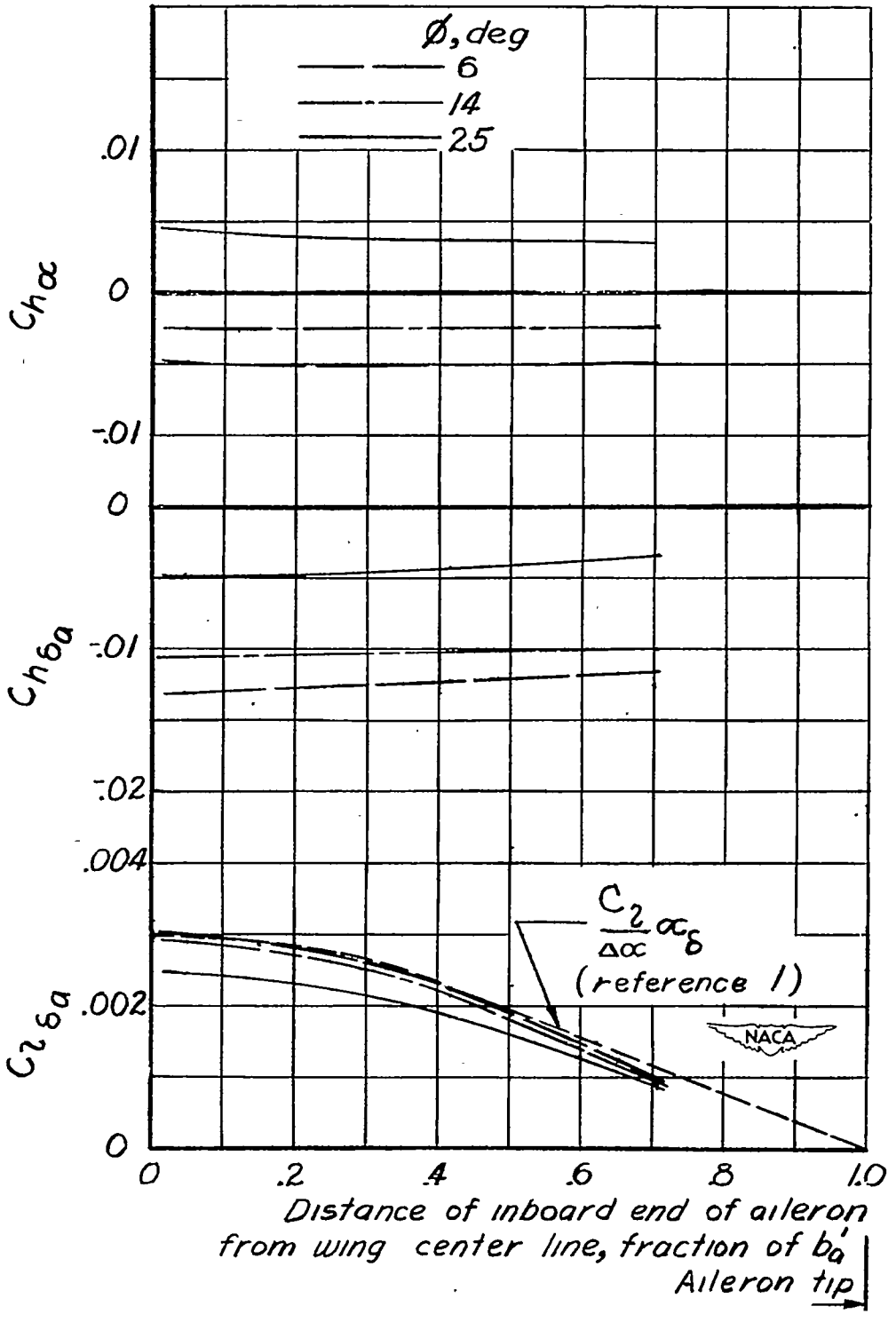

Figure 17.- Variation of aileron parameters $C_{l_{\delta a}}$, $C_{h_{\delta a}}$, and C_{h_α} with relative position of inboard end of aileron for three trailing-edge angles.

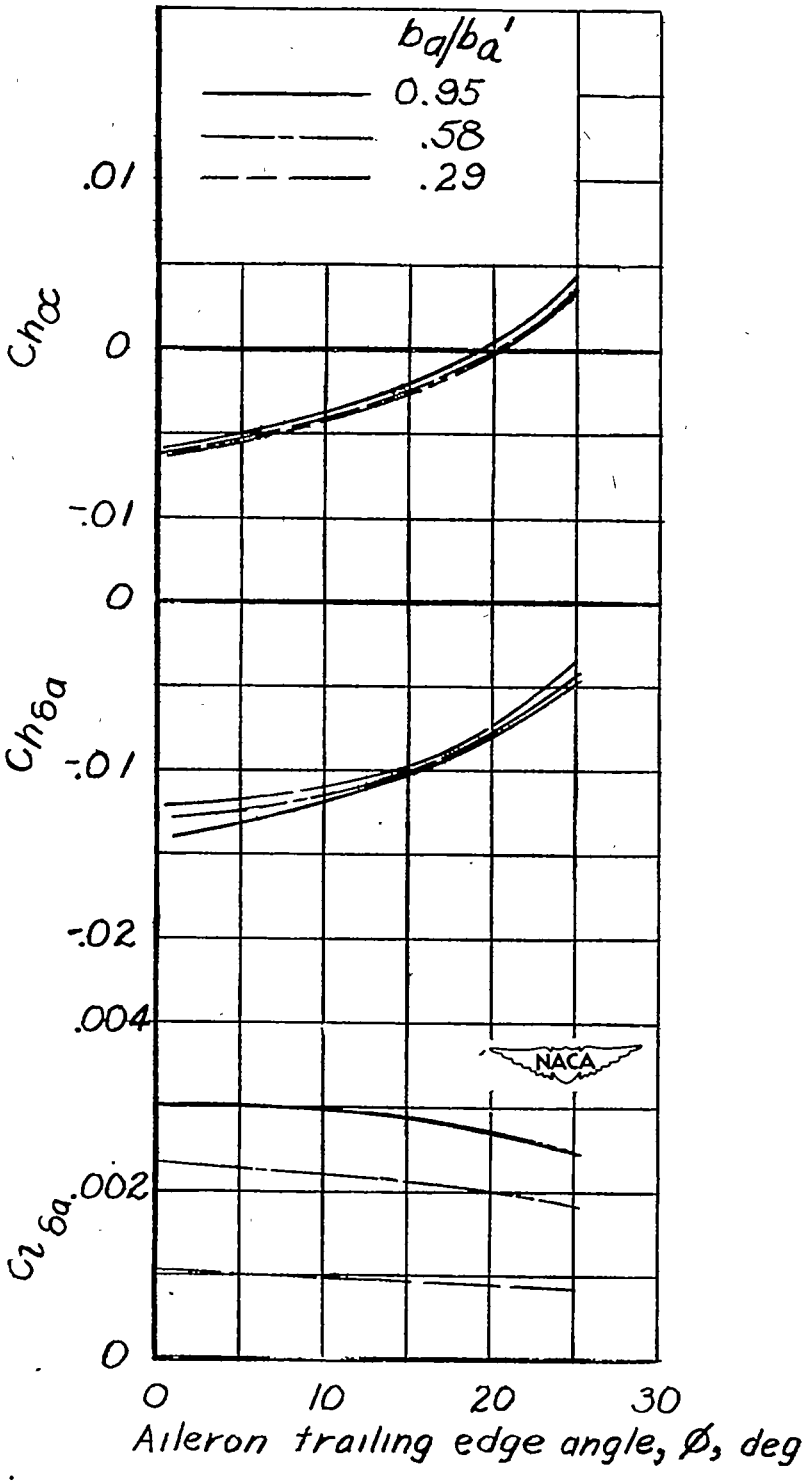

Figure 18.- Variation of aileron parameters $C_{l_{\delta_a}}$, $C_{n_{\delta_a}}$, and C_{h_α} with aileron trailing-edge angle for three aileron spans.

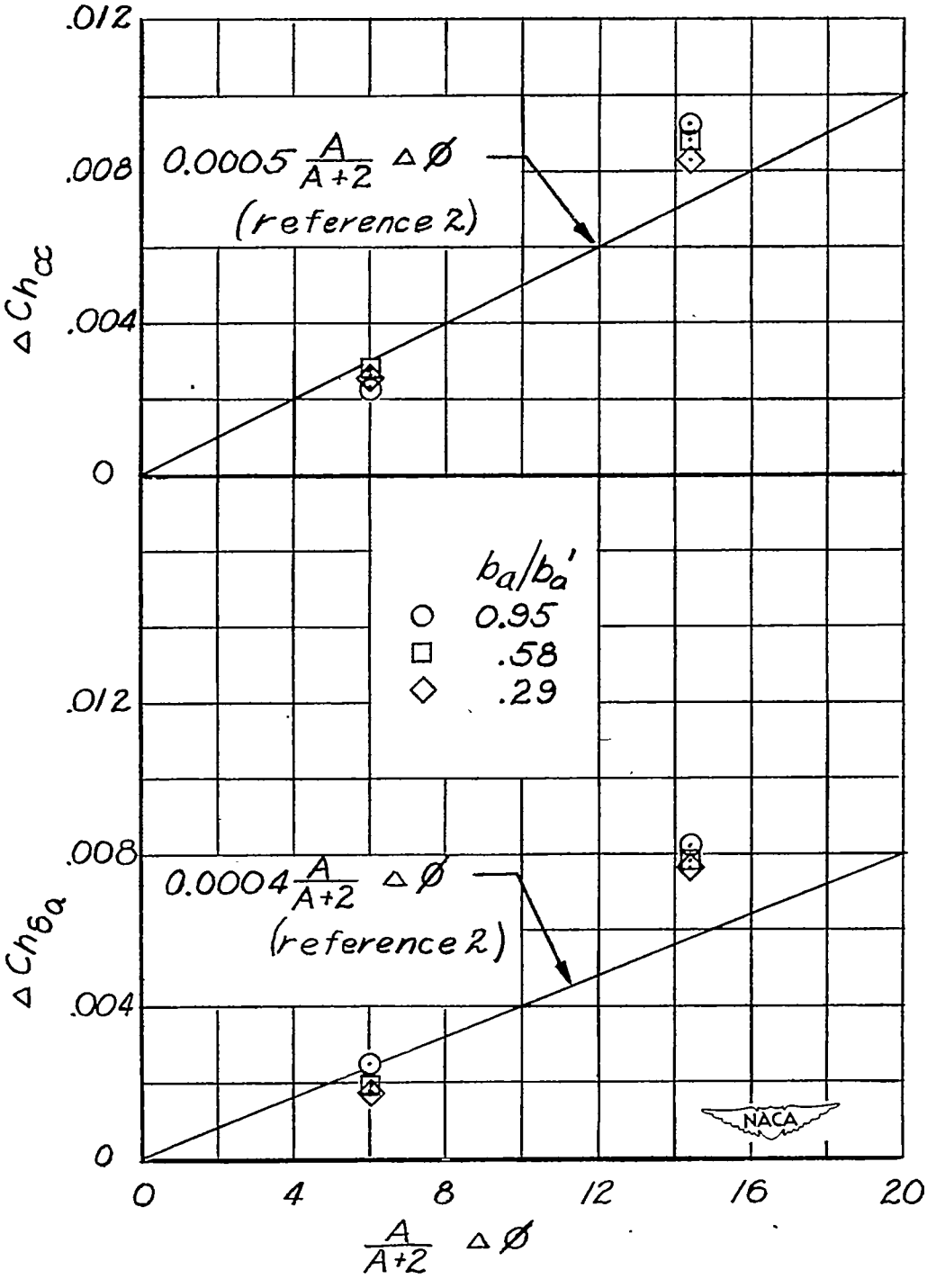

Figure 19.- Comparison of increments of hinge-moment parameters $C_{h_{\delta_a}}$ and C_{h_α} measured on semispan wing model with empirical curve presented in reference 2.